


# The meaning of carbonate Zn isotope records: Constraints from a detailed geochemical and isotope study of bulk deep-sea carbonates

## Journal Article

### Author(s):

Müsing, Kim ; Clarkson, Matthew O.; Vance, Derek

### Publication date:

2022-05-01

### Permanent link:

<https://doi.org/10.3929/ethz-b-000538302>

### Rights / license:

[Creative Commons Attribution-NonCommercial-NoDerivatives 4.0 International](#)

### Originally published in:

Geochimica et Cosmochimica Acta 324, <https://doi.org/10.1016/j.gca.2022.02.029>

### Funding acknowledgement:

165904 - Metal isotope constraints on biosphere-environment interactions in Earth history (SNF)

184873 - Using trace metal isotopes to understand ocean biogeochemistry: ancient and modern (SNF)

795722 - How does the Earth stop global warming? Using metal isotopes to understand climate recovery processes (EC)



# The meaning of carbonate Zn isotope records: Constraints from a detailed geochemical and isotope study of bulk deep-sea carbonates

Kim Müsing\*, Matthew O. Clarkson, Derek Vance

*Institute of Geochemistry and Petrology, Department of Earth Sciences, ETH Zürich, Clausiusstrasse 25, 8092 Zürich, Switzerland*

Received 13 July 2021; accepted in revised form 26 February 2022; available online 4 March 2022

## Abstract

Studies of the zinc isotope ( $\delta^{66}\text{Zn}$ ) composition of the past ocean often exploit the bulk carbonate sediment as an archive. The relationship of bulk carbonate  $\delta^{66}\text{Zn}$  to seawater values, however, is poorly understood. Experimental results suggest that inorganic carbonate records  $\delta^{66}\text{Zn}$  that is substantially higher than the aqueous  $\text{Zn}^{2+}$  pool. On the other hand, biogenic carbonate from modern cold-water corals and benthic foraminifera appear to record the ambient seawater  $\delta^{66}\text{Zn}$  value, without fractionation. Here, we address this problem through a detailed study of the different geochemical and isotope reservoirs in deep-sea carbonate samples.

Carbonate-rich, pelagic sediment samples were used in this study, one of Holocene age and one from the mid-Cretaceous. The samples were subjected to extensive leaching experiments and interpreted using a mixing model to identify silicate and Fe-Mn oxide contaminants as well as pure carbonate phases. The chemical and isotopic characteristics of the contaminant phases are consistent with previous analyses of silicates and Fe-Mn oxides. The  $\delta^{66}\text{Zn}$  values of the pure carbonate end-members, identified using a mixing model, at +0.93 to +1.10‰, are within analytical uncertainty of results obtained via leaching with buffered 1 M acetic acid (pH 5). By contrast, the  $\delta^{66}\text{Zn}$  of un-buffered acetic acid leachates are up to 0.35‰ beneath these values, reflecting the influence of contaminant phases. Weak mineral acids (e.g. 0.2–0.5 M HCl) are lighter still, at up to 0.5‰ below carbonate end-members.

The bulk carbonate sediment end-member  $\delta^{66}\text{Zn}$  for the Holocene sample are  $\sim 0.37\text{--}0.54\%$  above deep ocean values, consistent with the experimentally determined isotope offset between inorganic carbonate precipitates and an aqueous fluid. These carbonate end-members do not appear to directly record seawater compositions, unlike some biogenic carbonates. These differences identify the potential for ancient sediment  $\delta^{66}\text{Zn}$  records to reflect variations in Zn incorporation mechanism into the carbonate, rather than the  $\delta^{66}\text{Zn}$  of contemporary seawater, and hence may not reflect changes in Zn sources and sinks driven by environmental change. Further research is required to better identify the controls of  $\delta^{66}\text{Zn}$  in bulk carbonate sediments to reliably use them as an archive for seawater.

© 2022 The Authors. Published by Elsevier Ltd. This is an open access article under the CC BY-NC-ND license (<http://creativecommons.org/licenses/by-nc-nd/4.0/>).

**Keywords:** Deep-sea carbonates; Bulk carbonate sediments; Zinc; Zn isotopes; Geological archive; palaeoceanography; Selective leaching; Reductive cleaning

## 1. INTRODUCTION

The potential of transition metal stable isotope systems as tracers of Earth System processes has been facilitated by both analytical and conceptual developments over the

\* Corresponding author.

E-mail address: [kim.muesing@erdw.ethz.ch](mailto:kim.muesing@erdw.ethz.ch) (K. Müsing).

past decade (see, for example, reviews in Moynier et al., 2017; Kendall et al., 2017; Andersen et al., 2017). These developments have markedly improved our understanding of the metal that is our focus here, zinc (Zn) (e.g. Maréchal et al., 1999; Bermin et al., 2006; John and Conway, 2014; Little et al., 2014a, 2016; Zhao et al., 2014; Conway and John, 2015; Vance et al., 2016; Weber et al., 2018; Lemaitre et al., 2020). As evidenced by the modern Black Sea, both the abundances and the isotope compositions of Zn are impacted by dissolved sulphide (Vance et al., 2016). But Zn is also an important nutrient for phytoplankton growth (Morel and Price, 2003) and thus has much lower dissolved concentrations in the photic zone than in the deep ocean (e.g. Bruland et al., 1980; Lohan et al., 2002). An increasing number of studies seek to apply this knowledge to understand biogeochemically important aspects of the past ocean, such as redox and primary productivity (e.g. Kunzmann et al., 2013; John et al., 2017; Liu et al., 2017; Isson et al., 2018; Sweere et al., 2018; Chen et al., 2021).

Such studies of the ancient oceans require a reliable geological archive, one that is as temporally and geographically ubiquitous as possible, so that information can be obtained on global scales and with stratigraphic continuity. Marine carbonates have proven to be useful recorders of many fundamental aspects of the past chemistry of the oceans, e.g. via oxygen and carbon isotopes (e.g. Curry et al., 1988; Lea, 2014 and references therein), trace element contents (e.g. Barker et al., 2005), and novel isotopic tracers including metal isotopes (e.g. Li, B, Mo, U: Voegelin et al., 2009; Pogge von Strandmann et al., 2013; Penman et al., 2014; Clarkson et al., 2018). Particular advantages of carbonates include their near-continuous record from the Archean onwards, their importance to the fossil record so that biogeochemical information can be tied to biological evolution, and a link to contemporaneous seawater chemistry that has the potential to be simpler than for other chemical sediments (Boyle, 1981; Marchitto et al., 2000; Pichat et al., 2003).

However, there are also obstacles to be overcome, practical and conceptual, before carbonate records of past seawater isotopes can be robustly interpreted. The main conceptual issue concerns the relationship between the original dissolved isotope composition of seawater and that transferred to carbonate. Recent experimental studies have found that Zn isotopes fractionate significantly, and in a rather consistent manner, in the process of incorporation into and adsorption onto inorganic calcite (Dong and Wasylenki, 2016; Mavromatis et al., 2019). By contrast, Zn isotope measurements of cold-water corals and foraminifera, have returned values identical to modern seawater (Little et al., 2021; Druce et al., 2022). Given this variability, the meaning of Zn isotope values, and secular trends, that have been published for ancient carbonate (Pichat et al., 2003; Kunzmann et al., 2013; John et al., 2017; Liu et al., 2017; Sweere et al., 2018; Chen et al., 2021) is unclear.

The second issue is practical. Carbonate sediments and rocks consist not only of pure carbonate components, but also so-called “contaminant phases”, such as clays,

ferromanganese-oxide coatings, organic matter and detrital silicate, all of which contain distinct metal isotope signatures that are different from seawater (for Zn see review in Moynier et al., 2017). A simple bulk analysis of a carbonate sample is likely to return metal isotope data that are difficult to interpret in terms of past seawater, depending on the degree of contamination. It is, therefore, desirable to avoid these different contaminant phases through dissolution protocols that, so far as possible, target the carbonate only (e.g. Tessier et al., 1979; Boyle, 1981). Of particular concern are Fe-Mn oxyhydroxides, present in all marine sediments deposited in oxic environments, highly enriched in trace metals relative to the carbonate fraction (e.g. Manheim and Lane-Bostwick, 1991; Koschinsky and Hein, 2003), and often strongly fractionated relative to seawater (e.g. Maréchal et al., 2000; Little et al., 2014a; 2014b).

Previous studies of trace metal isotopes in bulk carbonate sediment samples have commonly used weak organic acids (acetic; e.g. Pichat et al., 2003; Kunzmann et al., 2013; Sweere et al., 2018) or dilute mineral acids (HCl or HNO<sub>3</sub>; e.g. Brennecke et al., 2011; Romaniello et al., 2013; Zhang et al., 2019) to selectively extract the carbonate phase, including the incorporated metals. These non-aggressive leaching solutions are typically assumed to yield negligible amounts of metals from contaminant phases, although detailed methodological studies have generally not been published (e.g. Pichat et al., 2003; Kunzmann et al., 2013; John et al., 2017; Liu et al., 2017). Most studies of Zn isotopes have used dilute unbuffered acetic acid, with concentrations ranging from 0.05 M to 2 M, sometimes involving heating, sometimes at room temperature (Pichat et al., 2003; Kunzmann et al., 2013; John et al., 2017; Liu et al., 2017; Sweere et al., 2018; Zhao et al., 2021). However, to date no extensive assessment has been made of the effects that different acids and acid strengths in the leaching solution have on carbonate-bound trace metals, particularly for Zn isotopes.

By contrast, studies aiming to shed light on Quaternary ocean chemistry via marine carbonate sediments have typically applied reductive cleaning techniques to remove ferromanganese oxide coatings from handpicked foraminiferal tests, ostracods and corals, prior to the carbonate dissolution step (e.g. Boyle, 1981; Boyle and Keigwin, 1985; Marchitto et al., 2000). The procedure typically involves a solution that contains hydrous hydrazine to reduce the Fe-Mn-oxides, followed by dissolution with weak acid to obtain the purest possible carbonate fraction (Boyle, 1981; Boyle and Keigwin, 1985). Chemical pre-cleaning is essential for producing reliable foraminiferal trace metal records, and physical removal of coatings has been shown to be required to obtain primary carbonate Zn isotope records in corals (Little et al., 2021). Whilst the physical separation of biogenic carbonates is possible for younger sediments, lithified samples require the use of bulk leaching techniques. The efficacy of reductive cleaning on removing contaminant phases has very recently also been assessed for bulk archives (Druce et al., 2022).

In order for these conceptual and practical issues to be addressed, systematic studies of modern and ancient

carbonate are required. These studies need to address the relationship between modern seawater and carbonate Zn isotopes (c.f. Zhao et al., 2021; Little et al., 2021), but also the efficacy of different extraction techniques aimed at isolating pure carbonate Zn isotopes and the potential for contamination by other phases. In this study, we present the results of detailed leaching experiments with a recent and an ancient carbonate sample with the following objectives: (1) to better understand the relationships between modern seawater Zn isotopes and those incorporated into carbonate; (2) to investigate the necessity and efficacy of established pre-dissolution reductive cleaning procedures (e.g. Boyle 1981; Clarkson et al., 2020) for bulk carbonate sediments in order to obtain Zn isotope signatures unbiased by metal oxide and exchangeable contaminants; (3) to compare the effects of different dissolution protocols on Zn isotope results; (4) to isolate potential contaminants of the carbonate signal and to assess their impact. A companion paper (Clarkson et al., 2020) has recently presented the results of a similar study for U and Mo in marine carbonates, using the same approach, on the same samples, and using analytical solutions derived from the same leaching experiments.

## 2. SAMPLES AND METHODS

### 2.1. Samples

The pelagic carbonate samples used in this experimental study were chosen to represent a recent and an ancient marine sediment sample. The same samples were the subjects of the detailed Mo-U study in Clarkson et al. (2020). The recent (Holocene) sample (4.4–6.4 kyr; Burton and Vance, 2000) was retrieved from ODP (Oceanic Drilling Program) site 758 (Leg 121, Core 001H, Sect 01 W, Interval 9–12 cm) in the Bay of Bengal, north-east Indian Ocean. The interval analysed here consists mainly of biogenic calcium carbonate (61%; Clarkson et al., 2020), and consists of nannofossil ooze with foraminifers with additional silts and clays (Peirce et al., 1989). Diagenetic manganese carbonate overgrowths and cements have been observed on planktonic foraminifera tests and the occurrence of Mn-oxide coatings has been confirmed (Burton and Vance, 2000). The peak Mn concentrations, however, occur at depth intervals beneath that studied here (Burton and Vance, 2000).

The ancient hemipelagic, organic-deficient limestone sample, GA183, from the Gongzha section in Tibet, was deposited in the mid-Cretaceous under oxic water-column conditions, though conditions were probably reducing beneath the sediment-water interface (Bomou et al., 2013; Li et al., 2017; Clarkson et al., 2020; Chen et al., 2021). This section was recently part of a Zn isotope study by Chen et al. (2021), and their sample TOC56 represents the same stratigraphic level as sample GA183 studied here. The sample primarily consists of carbonate (planktonic foraminifera, calcareous nanofossils, ~70%; Clarkson et al., 2020) and detrital silicates. For ease of reference, we henceforth refer to these two samples as “Holocene” and “Cretaceous”.

### 2.2. Cleaning and dissolution protocol

All the trace metal elemental abundance and isotope work was carried out in Class 10 laminar flow workstations within Class 1000 clean laboratories of the Institute of Geochemistry and Petrology at ETH Zürich. All reagents used were either purified through sub-boiling distillation or ion exchange methods, or purchased as ultra-pure grade. Deionized water (18.2 M $\Omega$ ), purified with a Millipore System (Milli-Q, Merck Millipore) was used for preparation of all solutions. Pre-cleaned Savillex PFA labware products were used throughout the chemical separation procedures.

For each bulk carbonate sediment sample, 20 aliquots of 180–230 mg homogenized sample powder were rinsed three times with MilliQ H<sub>2</sub>O (>18.2 M $\Omega$ ). For the samples labelled “uncleaned” no further pre-cleaning was done. Half of the samples were subjected to reductive cleaning (“cleaned” samples), with 10 ml of a solution containing 1 M hydrous hydrazine and 0.25 M citric acid in 16 M ammonium hydroxide to remove Fe-Mn-oxide coatings. This approach is based on protocols widely used to clean handpicked foraminifera tests (Boyle and Keigwin, 1985), including to extract foraminiferal Zn/Ca ratios (e.g. Marchitto et al., 2002), and is comparable to cleaning treatments recently applied to cold-water corals by Little et al. (2021). The samples were cleaned for 30 min in a hot water bath (~90 °C), with manual agitation every few minutes. After the cleaning step, the reductive solution was removed and discarded, and the samples were rinsed and centrifuged a further three times with MilliQ to remove traces of the cleaning solution.

Different dissolution protocols investigated the acids commonly used to selectively extract carbonate, as well as higher strength acids in order to characterise the isotopic signal from different potential contaminant phases. For each bulk carbonate sediment sample, uncleaned and cleaned sample pairs were each dissolved with 5–10 ml unbuffered 0.2 M and 1 M acetic acid, 1 M acetic acid, buffered (to pH 5) with either sodium acetate (NaOAc) or ammonium acetate (NH<sub>4</sub>OAc), 0.2 M, 0.5 M, 1 M, 3 M, 7 M hydrochloric acid (HCl) and 3 M nitric acid (HNO<sub>3</sub>) (Clarkson et al., 2020). The acetic based extractions were performed at room temperature, with constant agitation for 24 h. All HCl and HNO<sub>3</sub> extractions were done at room temperature for 1 h, and further sample pairs for ODP 758 were treated with 0.2 M, 1 M and 3 M HCl for 24 h. For comparison, published carbonate trace metal isotope studies typically use durations from 10 min to 24 h, at room temperature to 70 °C (e.g. Pichat et al., 2003; Liu et al., 2017; Zhang et al., 2019). The pH was measured at the beginning and end of the leaching experiments. In nearly all cases pH remained the same – 5 for the buffered leachates, 0–0.5 for the HCl and HNO<sub>3</sub> based leachates (see Clarkson et al., 2020). The only exceptions were the 0.2 M acetic acid and 0.2 M HCl leachates, where the pH increased by around 3 units during the experiment.

Selected sample residues after leaching (35–60 mg) as well as bulk samples (60 mg) were digested for analysis using a mixture of concentrated HF and HNO<sub>3</sub> and heating

on a hotplate (130–140 °C, 48 h) or in a high pressure PAAR bomb (210 °C, 24 h). Following this digestion, clear solutions with no residues were obtained. Acetic based leachates were oxidized and dried down with excess concentrated HNO<sub>3</sub>, whilst HCl and HNO<sub>3</sub> leachates were simply dried down. The salt precipitates were then converted to chloride form with 7 M HCl, dried and re-dissolved in 1 ml 7 M HCl + H<sub>2</sub>O<sub>2</sub> ready to load on columns.

### 2.3. Chemical purification

The sample leachates were collected for purification via column chromatography. Prior to column chromatography, a <sup>64</sup>Zn-<sup>67</sup>Zn spike (Bermin et al., 2006) was added to aliquots of each solution, with a sample/spike ratio of close to 1, to correct for mass fractionation during the chemical purification procedure or mass spectrometric analysis. The spiked Zn sample fractions were purified using two passes through an anion exchange column (BioRad macroporous AG MP-1; Archer and Vance, 2004; Bermin et al., 2006). The pure Zn fractions were oxidized for at least 24 h with concentrated H<sub>2</sub>O<sub>2</sub> and HNO<sub>3</sub>, and re-dissolved in 2% HNO<sub>3</sub> for isotope analysis. Typical Zn blanks for the purification procedure were found to be around 1.2 ng. This value is negligible compared to the smallest sample size (825 ng) and no blank correction was applied.

### 2.4. Mass spectrometry

Major and trace element concentration measurements were performed on a small aliquot of each experimental solution, on a Thermo Scientific ELEMENT2/XR magnetic sector inductively coupled plasma source mass spectrometer (ICP-MS). An indium (In) standard was added to the samples beforehand to monitor and correct for instrumental instabilities. The results were blank-corrected, and an in-house standard resembling the composition of foraminiferal calcite was used as a primary concentration standard. A secondary carbonate standard, measured repeatedly together with the samples yielded a reproducibility of ±8% (2SD, n = 9) for Zn/Ca.

The isotopic composition of Zn was measured on a Thermo Scientific NEPTUNE Plus multi-collector ICPMS, using methods detailed in previous studies, including mass bias correction using the double spike approach (Little et al., 2014a). Solutions containing ~100 ppb of Zn were introduced in 2% HNO<sub>3</sub> via a Cetac Aridus II desolvating nebulizer system with a PFA nebuliser (50 µL·min<sup>-1</sup>) and spray chamber. The applied data reduction methods are described by Siebert et al. (2001). The Zn isotope ratios are reported in the standard delta notation relative to JMC-Lyon:

$$\delta^{66}\text{Zn} = \left[ \left( \frac{{}^{66}\text{Zn}/{}^{64}\text{Zn}}{\text{sample}} \right) / \left( \frac{{}^{66}\text{Zn}/{}^{64}\text{Zn}}{\text{JMC-Lyon}} - 1 \right) \right] \times 1000$$

Early in this study our JMC-Lyon primary standard ran out and a new standard, AA-ETH Zn, was introduced. This has a  $\delta^{66}\text{Zn}$  value of  $+0.28 \pm 0.02\text{‰}$  (n = 110, 2SD) relative to the formerly used JMC-Lyon (Archer et al., 2017; Lemaitre et al., 2020). A secondary Zn standard IRMM-

3702 was measured repeatedly to track long-term external reproducibility, and yields  $\delta^{66}\text{Zn} = +0.30 \pm 0.06\text{‰}$  (n = 197, 2SD). The internal uncertainties for the Zn isotope results are all smaller than the external reproducibility, so that the latter will be used as the true uncertainty.

## 3. RESULTS

Elemental and isotope data for the Holocene sample (ODP 758) and the Cretaceous sample (GA183) are presented in Tables 1 and 2. Clarkson et al. (2020) reported the total carbonate contents of these samples at 61% and 70%, respectively. Fig. 1 uses the measured Ca concentration of the leachates (Tables 1 and 2) and the assumption that the carbonate in the samples is stoichiometric CaCO<sub>3</sub> to assess the proportion of this total that was extracted by the different leachates. For uncleaned samples, 86 ± 9% (Holocene sample, 1SD) and 96 ± 15% (Cretaceous sample) of the carbonate in the two samples is extracted by the leaching acids, with a tendency for the lower molarity acids (both acetic and HCl) to extract the least carbonate. Leachates of the cleaned samples yield much lower proportions of the total carbonate, at 49 ± 6% and 72 ± 13% for the Holocene and the Cretaceous sample, respectively, reflecting the fact that significant carbonate dissolution occurs during the reductive cleaning step due to the presence of citric acid as a chelating agent (Clarkson et al., 2020).

### 3.1. Elemental abundances

Because of carbonate dissolution during reductive cleaning, and because samples were not re-weighed after cleaning, absolute concentrations of Zn and other elements are not available for the final cleaned sample. Element/Ca ratios, on the other hand, are not impacted by this issue so that throughout the rest of the paper elemental abundances are discussed in terms of these ratios.

For the Holocene sample (Table 1, Fig. 2), the three least aggressive leaching reagents – 0.2 M acetic acid or buffered 1 M acetic acid – yield significantly lower Al/Ca (and Fe/Ca ratios, Table 1) than any other leaching or digestion approach. There is then a step up to the unbuffered 1 M acetic acid, after which there is a more gradual, and more or less monotonic, increase with more aggressive leaching approaches: stronger reagents and longer reaction time – 24 h versus 1 h – also yield higher Al/Ca and Fe/Ca. The most aggressive leaching approaches return Al/Ca (up to 40,000 µmol/mol) and Fe/Ca (up to 28,000 µmol/mol, Table 1) that are still well below those obtained from the total or bomb digest (170,000 and 47,000 µmol/mol, respectively). A further important feature of the Al/Ca and Fe/Ca data is that cleaned samples always have higher values than uncleaned samples.

For Mn/Ca in the uncleaned samples, the pattern with increasingly aggressive leaching is similar to the above but, in contrast to Al/Ca and Fe/Ca, the Mn/Ca of the strongest leaching acids is very close to the total digest (Fig. 2, 2300 versus 2500 µmol/mol). The data patterns in Mn/Ca for samples that had been reductively cleaned

Table 1  
Concentration and isotope data for leachates and bulk dissolution of Holocene sample ODP 758.

Sample name	Leaching time (h)	Ca <sup>1,2</sup> (wt.%)	Mn/Ca (μmol/mol)	Al/Ca (μmol/mol)	Fe/Ca (μmol/mol)	Zn/Ca (μmol/mol)	δ <sup>66</sup> Zn (‰)	2SE <sup>3</sup> (‰)
<b>Samples with no prior reductive cleaning</b>								
0.2 M acetic	24	19.4	218	244	30.2	13.4	1.25	0.03
1 M NaOAc	24	25.1	295	815	26.9	39.4	0.85	0.04
1 M NH <sub>4</sub> Ac	24	21.1	321	890	25.9	58.4	0.82	0.04
1 M acetic	24	19.9	435	3180	197	68.2	0.71	0.03
0.2 M HCl	1	18.7	402	3240	8.64	69.2	0.79	0.04
0.5 M HCl	1	21.1	848	11,400	2120	101	0.57	0.03
1 M HCl	1	21.2	1040	11,900	2870	95.2	0.50	0.03
3 M HCl	1	20.8	1990	13,800	5360	109	0.46	0.04
7 M HCl	1	21.5	2130	17,000	10,300	121	0.40	0.03
3 M HNO <sub>3</sub>	1	21	1220	14,000	4100	102	0.48	0.03
0.2 M HCl	24	25.2	625	4510	13.3	62.5	0.68	0.05
1 M HCl	24	16.9	2300	19,800	11,200	204	0.33	0.04
3 M HCl	24	19.3	2500	32,400	22,500	199	0.39	0.05
Total Digest		24.8	2500	1.7 × 10 <sup>5</sup>	41,600	198	0.32	0.04
Bomb		25.6	2500	1.6 × 10 <sup>5</sup>	47,200	223	0.31	0.05
1 M NaOAc residue		0.3	55,000	51 × 10 <sup>7</sup>	1.0 × 10 <sup>7</sup>	13,300	0.17	0.03
1 M NH <sub>4</sub> Ac residue		0.3	1.5 × 10 <sup>5</sup>	1.1 × 10 <sup>7</sup>	3.0 × 10 <sup>6</sup>	10,700	0.10	0.04
3 M HCl residue		0.7	1.7 × 10 <sup>5</sup>	1.4 × 10 <sup>7</sup>	3.2 × 10 <sup>6</sup>	11,000	0.08	0.07
7 M HCl residue		0.3	17,000	1.0 × 10 <sup>7</sup>	2.4 × 10 <sup>6</sup>	4310	0.19	0.04
<b>Samples reductively cleaned prior to leaching</b>								
0.2 M acetic	24	12.8	548	1420	324	57.3	0.93	0.04
1 M NaOAc	24	12.3	517	1950	156	60.2	0.81	0.03
1 M NH <sub>4</sub> Ac	24	11.6	548	1860	172	95.0	0.79	0.03
1 M acetic	24	14.3	603	5530	1120	118	0.67	0.04
0.2 M HCl	1	12.7	603	14,700	1840	138	0.56	0.03
0.5 M HCl	1	12.7	614	17,000	2970	145	0.50	0.03
1 M HCl	1	12.2	623	17,600	3710	147	0.47	0.03
3 M HCl	1	12.4	639	20,100	6590	158	0.43	0.03
7 M HCl	1	11	723	25,800	16,000	181	0.38	0.03
3 M HNO <sub>3</sub>	1	12	651	19,500	4870	144	0.49	0.03
0.2 M HCl	24	12.7	664	19,900	5330	193	0.34	0.06
1 M HCl	24	10.8	718	29,300	15,400	212	0.30	0.06
3 M HCl	24	7.6	848	42,400	28,000	250	0.31	0.05

<sup>1</sup> Ca concentrations given here and in Table 2 are relative to the initial weight of the sample aliquot leached.

<sup>2</sup> Mn/Ca, Al/Ca and Fe/Ca ratios of GA183 and ODP 758 have already been reported in Clarkson et al. (2020).

<sup>3</sup> Two standard errors of the mean of 30 isotope ratio analyses in one analysis, fully propagated through the double spike reduction procedure.

before leaching are different in several significant ways (Fig. 2). First, there is much less variability in response to increasing reagent strength and reaction time. Second, while Mn/Ca ratios for the least aggressive leachates are also higher for cleaned than uncleaned samples, the opposite is true for leaching reagents stronger than 1 M HCl. Third, the highest Mn/Ca ratio obtained from the most aggressive leachates of cleaned samples (850 μmol/mol) is well below that obtained from the total digest (2500 μmol/mol).

As for Al/Ca and Fe/Ca, leaching experiments on cleaned samples yield higher Zn/Ca than uncleaned samples (Table 1, Fig. 2), and Zn/Ca increases with acid strength (Zn/Ca = 13–180 μmol/mol). The strongest acid, 7 M HCl, yields the highest Zn abundances in the 1 h experiments, and the 24 h reaction time always releases more Zn relative to Ca. Finally, for both cleaned and uncleaned samples the most aggressive leaching approaches yield Zn/

Ca ratios that are close to those obtained from the total digest (Fig. 2).

The Cretaceous carbonate (Table 2) contains much less Al, Mn and Zn than the Holocene sample (Fig. 2). Al/Ca ratios also increase with increasingly aggressive leaching approaches, but reach a maximum that is about an order of magnitude less than the modern sample. Like the Holocene sample, this maximum (~7000 μmol/mol) is far below the Al/Ca of the total digest (90,000 μmol/mol). Also like the Holocene sample, there is very little variability in Mn/Ca in response to increasing reagent strength and reaction time, but in this case this observation applies to both cleaned and uncleaned samples. The Mn/Ca ratio obtained by leaching, whether on cleaned or uncleaned samples, is close to that of the bulk digest (Fig. 2). Most leachates have Zn/Ca ratios < 2 μmol/mol, but those obtained for stronger reagents are again higher, reaching a maximum of around 15–20 μmol/mol for 7 M HCl (Table 2). The pattern of

Table 2

Concentration and isotope data for leachates and bulk dissolution of Cretaceous sample GA183.

Sample name	Leaching time (h)	Ca <sup>1,2</sup> (wt.%)	Mn/Ca (μmol/mol)	Al/Ca (μmol/mol)	Fe/Ca (μmol/mol)	Zn/Ca (μmol/mol)	δ <sup>66</sup> Zn (‰)	2SE <sup>3</sup> (‰)
<b>Samples with no prior reductive cleaning</b>								
0.2 M acetic	24	21.5	802	158	3560	1.13		
1 M NaOAc	24	27.3	766	279	5370	1.02		
1 M NH <sub>4</sub> Ac	24	26.3	787	184	5470	1.34	1.10	0.02
1 M acetic	24	30.5	796	505	5870	1.38	0.96	0.03
0.2 M HCl	1	17.2	800	145	5200	1.44	1.02	0.02
0.5 M HCl	1	29.3	784	1580	6050	2.15	0.64	0.02
1 M HCl	1	28	786	1930	6200	2.56	0.54	0.02
3 M HCl	1	29.7	784	3230	7620	4.29	0.47	0.02
7 M HCl	1	29.4	777	7110	14,900	14.6	0.76	0.14
3 M HNO <sub>3</sub>	1	30.3	770	2650	7010	3.16	0.54	0.03
Total Digest Bomb		24.4	857	96,100	32,600	37.8	0.27	0.05
1 M NaOAc residue		31.1	868	91,200	43,200	46.5	0.19	0.04
3 M HCl residue		3.2	1450	$1.9 \times 10^6$	$7.2 \times 10^5$	950	0.28	0.06
7 M HCl residue		0.03	55,300	$2.1 \times 10^8$	$8.3 \times 10^7$	99,800	0.14	0.04
7 M HCl residue		0.03	5630	$5.0 \times 10^7$	$1.1 \times 10^7$	10,500	0.25	0.04
<b>Samples reductively cleaned prior to leaching</b>								
0.2 M acetic	24	20.2	814	78.7	2260	0.71	1.10	0.04
1 M NaOAc	24	19.7	770	141	5390	1.07	1.14	0.02
1 M NH <sub>4</sub> Ac	24	19.3	827	98.8	5840	1.08	1.09	0.03
1 M acetic	24	21.3	784	318	5750	1.38	0.93	0.02
0.2 M HCl	1	17.1	831	369	5870	1.42	0.88	0.02
0.5 M HCl	1	20.9	805	1330	6350	2.60		
1 M HCl	1	18.3	807	1740	6610	3.21		
3 M HCl	1	16.6	786	3250	7530	6.16	0.40	0.02
7 M HCl	1	18.6	819	7360	18,600	22.0	0.19	0.03
3 M HNO <sub>3</sub>	1	19.6	796	2540	6740	4.16	0.42	0.02

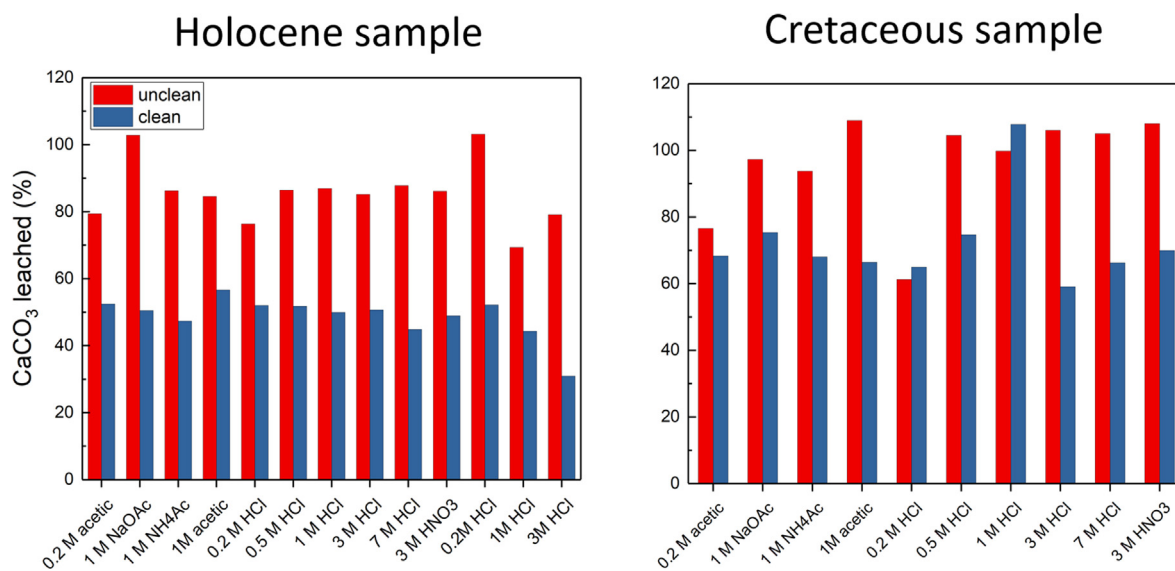


Fig. 1. Percentage of carbonate recovered by different leaching approaches applied to the two samples studied, given previously measured carbonate contents (Clarkson et al., 2020), measured Ca concentrations, and assuming that the carbonate is stoichiometric CaCO<sub>3</sub>. For the Holocene sample (ODP 758), the first set of data labelled 0.2 M, 1 M, 3 M HCl are 1 h experiments, the second set with these labels are 24 h experiments. In this and subsequent figures “unclean” denotes samples that were leached after rinsing with MQ only while “clean” denotes samples that were reductively cleaned prior to leaching.

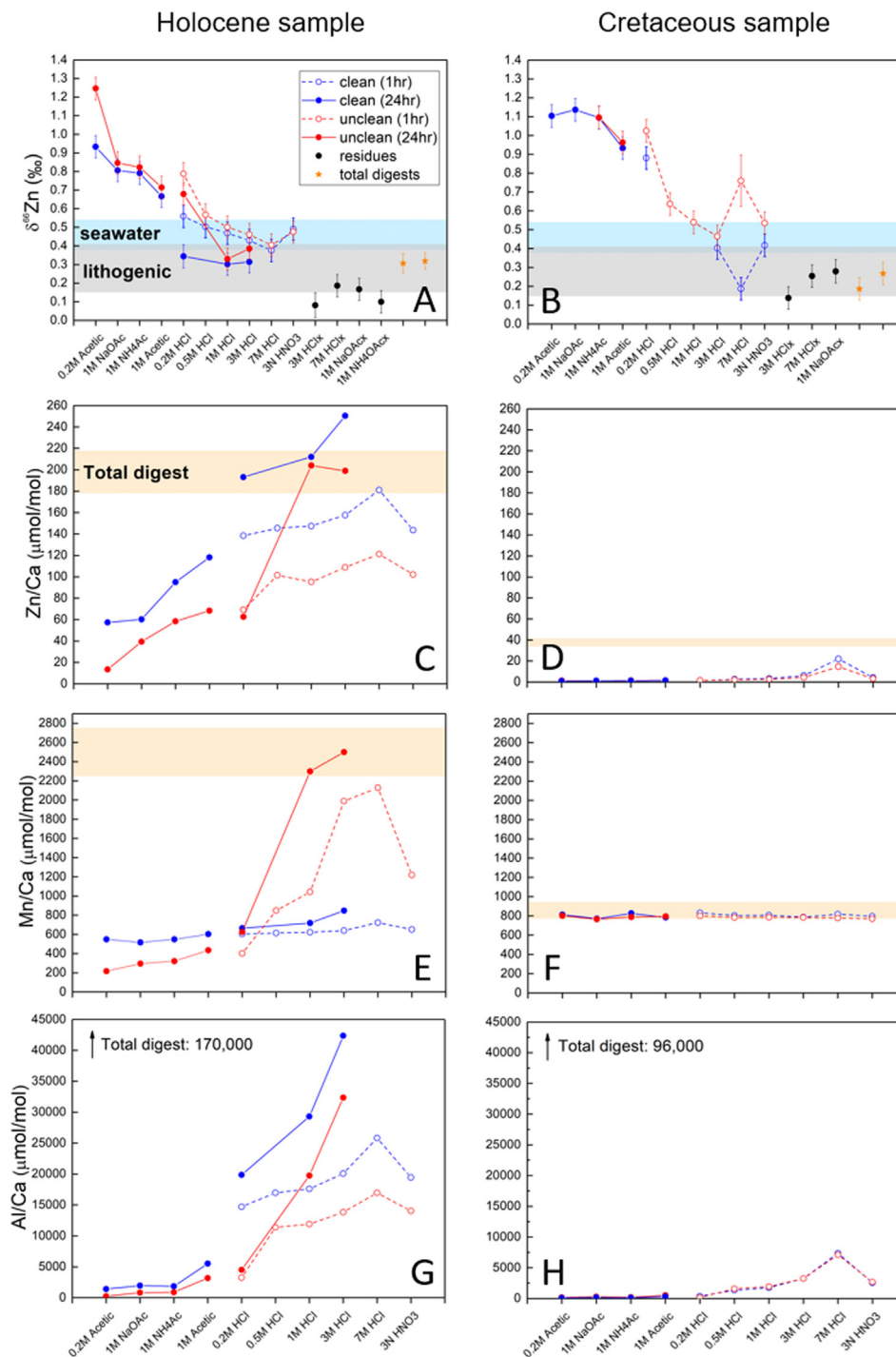


Fig. 2. Zinc isotope compositions and selected element/Ca ratios for the Holocene and the Cretaceous sample. Shaded bars in the element/Ca panels show the ratio extracted from the bulk sample by hotplate or bomb digestion with HF. Shaded bars in the isotope composition diagrams represent the isotope ranges for average lithogenic material (Moynier et al., 2017) and the modern deep ocean. The deep ocean range is an average and 1SD ( $+0.46 \pm 0.08\text{‰}$ ,  $n = 776$ ) of values reported in Boyle et al. (2012), Zhao et al. (2014), Conway and John (2014, 2015), Samanta et al. (2017), John et al. (2018), Wang et al. (2019), Vance et al. (2019), Sieber et al. (2020), Lemaitre et al. (2020). Data for the North Atlantic, where upper ocean variability extends lower, are for  $> 800$  m, everywhere else for  $> 500$  m. North Atlantic data show localised impacts from hydrothermal plumes and these data were excluded. In both the Pacific and the Atlantic, eastern margins also show anomalous values due to local processes and these data are also not included in the above compilation. Note that if all these data are included the resultant deep ocean value is  $+0.44 \pm 0.12\text{‰}$  ( $n = 814$ ), identical to that on the diagram but with a larger uncertainty.



variation across different leaching reagents is also different: Zn/Ca ratios remain uniformly low for the weak and the acetic acid-based leachates (0.7–1.4  $\mu\text{mol/mol}$ ), and only start increasing significantly for reagents stronger than 0.5 M HCl (Table 2).

### 3.2. Zinc isotopes

Zinc isotope data are presented for the two samples in Tables 1 and 2 and in Fig. 2, where they are compared to published data for the modern oceans and lithogenic isotope compositions.

The major feature of the Zn isotope data for both samples (Fig. 2A, B) is for heavier isotope compositions in the least aggressive leachates, with maxima at +1.25 and +1.10‰ for the cleaned Holocene and Cretaceous samples, respectively. Zinc isotope compositions decrease with more aggressive leaching methods and with longer reaction times. Zinc isotope data for the most aggressive leaching reagents (3 M HCl, 7 M HCl, 3 M HNO<sub>3</sub>) are nearly always in the range of the average lithogenic signature ( $+0.28 \pm 0.13\text{‰}$ ; Moynier et al., 2017), as is the bulk analysis. The above statements are generally true for both uncleaned and cleaned samples. But for the Holocene sample, the uncleaned samples always have slightly higher  $\delta^{66}\text{Zn}$ , by  $0.10 \pm 0.11$  (mean and 1 SD), although this difference is not always analytically significant. These features are much less clear in the Cretaceous sample, where the 7 M HCl leachate is the only sample with a significant difference between cleaned and uncleaned samples. Without a duplicate analysis, the significance of this latter result is not clear.

## 4. DISCUSSION

### 4.1. Constraints on metal reservoirs from element/Ca ratios

One objective of this paper is to assess the degree to which different cleaning and carbonate dissolution protocols can separate different reservoirs of trace metals within a bulk carbonate sediment sample. Most of the observations in the results section are consistent with mixing between at least three distinct reservoirs: carbonate, Fe-Mn oxide coatings and detrital silicates/clays.

Data arrays in element/Mn ratio space, as well as constraints from the literature for the chemistry of Fe-Mn oxide and silicate contaminants, serve to significantly clarify the nature of these reservoirs, and the mixing relationships between them (Fig. 3; further details of end-members and curve-fitting can be found in the appendix). We focus on the Holocene sample, where the different reservoirs mixing is more complex than for the Cretaceous sample. Cleaned and uncleaned analyses of the Holocene sample clearly separate into two different linear data arrays in Ca/Mn-Al/Mn space, that are each consistent with mixing between two end-members (Fig. 3A). The high Al/Mn end-member on Fig. 3A has Al-Mn-Ca characteristics similar to the suspended loads of large rivers (filled black square, Al/Mn = 106; Viers et al., 2009) and is likely a silicate. The data array for the uncleaned samples require

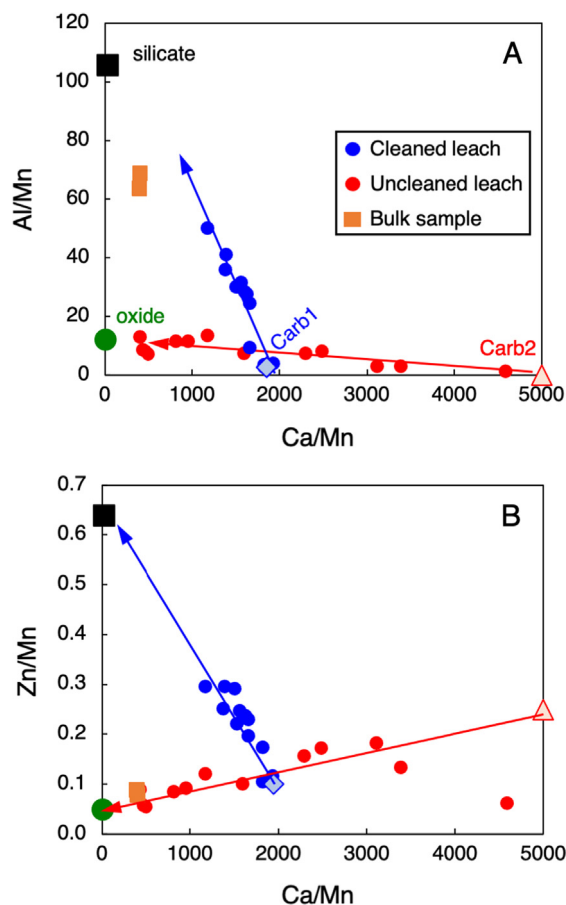


Fig. 3. Molar elemental ratio plots for the Holocene sample, showing data for leachates of previously reductively-cleaned samples, uncleaned samples, and bulk digests. In both panels, likely end-members whose mixing can explain the data are shown for silicate material (filled black square, particulate load of rivers from Viers et al., 2009), for Fe-Mn oxides (filled green circle; c.f. Little et al., 2021), and for two end-members with higher Ca/Mn (Carb1 and Carb2, blue diamond and red triangle) that are interpreted as carbonate phases. The Zn/Mn ratio for the silicate end-member that is consistent with a least-squares fit to the data in Fig. 3B is four times higher than the Zn/Mn ratio reported in Viers et al. (2009). Further details of the mixing calculations are given in the Appendix.

an end-member with a Ca/Mn ratio of zero and an Al/Mn ratio of 11.5 (filled green circle), consistent with physically-separated Fe-Mn oxide coatings on cold-water corals (Al/Mn = 0.1–20; Little et al., 2021).

These data arrays also require two end-members with high Ca/Mn, and with Al/Mn very close to zero, that likely represent different carbonate reservoirs. Most of the leachates are explained by mixing between end-member Carb1 (blue square, Ca/Mn = 1950 at Al/Mn = 0) and either the oxide (uncleaned) or silicate (cleaned) end-members as defined above. The exceptions are data for the least aggressive leaching approaches applied to uncleaned samples (all the acetic acid leachates as well as 0.2 M HCl), which lie at higher Ca/Mn than Carb1 and necessitate a fourth end-member at Carb2 (red triangle, Ca/Mn = 5000 at

Al/Mn = 0). It is theoretically possible that Carb1 is not a real end-member, and that it itself represents a mixture of Carb2 and oxide. This would, however, require that exactly the same proportions of Carb2 and oxide were extracted by the leaching of the cleaned samples for all leaching approaches, otherwise the data array defined by mixing towards silicate would be likely to be much less well defined.

The Ca/Mn ratios of the four end-members can be used in conjunction with the data arrays to define the Zn/Mn characteristics of the mixing end-members (Fig. 3B). The Zn/Mn ratio required of the metal-oxide end-member, of 0.05, is very close to those recently directly measured for Fe-Mn oxide coatings on cold-water corals (0.01–0.05, with one outlier at 0.6; Little et al., 2021). However, the Zn/Mn ratio of the end-member identified in Fig. 3A as silicate, given the Ca/Mn ratio of this end-member and the data array for the cleaned samples, must be a factor of about four higher (Zn/Mn = 0.64, filled black square in Fig. 3B) than that for suspended riverine particulates reported by Viers et al. (2009).

A prominent contrast between the two samples studied here is that, unlike the Holocene sample, Mn/Ca is invariant across all leachates of the Cretaceous sample – at the level of analytical uncertainty – while Al/Mn also shows much more subdued variations (Table 2). The small range in Mn/Ca for the Cretaceous sample is completely consistent with the previous suggestion that this sample appears to lack Fe-Mn oxide coatings (Clarkson et al., 2020). Diagrams such as those in Fig. 3 for the Holocene sample are not particularly useful for this Cretaceous sample, but we explore the ability of mixing between the phases identified above to explain the Zn isotope data for both samples in the next section.

#### 4.2. Zinc isotope compositions of reservoirs extracted by leaching

The main objective of this section is to investigate the degree to which mixing calculations can constrain the Zn isotope composition of the carbonate end-members and, in particular, to use these constraints to identify the best leaching approach to extract this Zn isotope composition. In addition, we seek to better understand the nature of the putative silicate and Fe-Mn oxide contaminants contributing to the leachates. Further details of these calculations are given in the appendix. Bearing in mind that the data we present derive from leaching experiments on a multi-phase bulk system, the isotope data conform remarkably well to the behaviour and patterns expected from mixing (Figs. 4, 5). Mixing hyperbolae defined by the Ca/Mn data provide the best constraints on the isotope composition of the two contaminants in the bulk sample. The required  $\delta^{66}\text{Zn}$  of the silicate end-member, at  $+0.14 \pm 0.15\text{‰}$ , is consistent with the average value for clastic sediments of  $+0.28 \pm 0.13\text{‰}$  (Moynier et al., 2017). Similarly, the  $\delta^{66}\text{Zn}$  of the oxide end-member in the uncleaned samples of the Holocene carbonate, at  $+0.20 \pm 0.15\text{‰}$ , overlaps with that directly measured for oxide coatings on cold-water corals ( $+0.47 \pm 0.21\text{‰}$ ; Little et al., 2021).

As noted in the previous section, the Holocene sample requires two separate carbonate phases, both with high but different Ca/Mn. The isotope compositions of these end-members are obtained from the point at which a least-squares fit to the data reaches the Ca/Mn ratio for these end-members as determined by Fig. 3. Using this approach, the  $\delta^{66}\text{Zn}$  of Carb2 is constrained to be  $+0.93 \pm 0.10\text{‰}$  from the Ca/Mn versus  $\delta^{66}\text{Zn}$  plot (see Appendix, Fig. 4A). The data for cleaned Holocene samples and for the Cretaceous sample do not yield as tight constraints on the  $\delta^{66}\text{Zn}$  of the corresponding carbonate end-members (Figs. 4, 5 and Appendix). However, for all mixing arrays, the least squares fit yields  $\delta^{66}\text{Zn}$  for the carbonate end-members that are within uncertainty of the value obtained via leaching with buffered acetic acid, whereas the values obtained from other leachates are significantly higher or lower. For example, the  $\delta^{66}\text{Zn}$  obtained using buffered acetic acid to leach the Holocene sample are  $+0.79$  to  $0.85\text{‰}$ , within analytical uncertainty of the value obtained for Carb2 from the mixing model of  $+0.93 \pm 0.10\text{‰}$ . Values obtained via leaching with unbuffered acetic acid extend from  $+0.67$  to  $+1.25\text{‰}$ . Using both the constraints from the mixing models and the data for the unbuffered acetic acids (Tables 1, 2), our best estimates of the  $\delta^{66}\text{Zn}$  of the carbonate end-members are:  $+0.93 \pm 0.10\text{‰}$  (Carb2),  $+0.90 \pm 0.10\text{‰}$  (Carb 1), and  $+1.10 \pm 0.05\text{‰}$  (Cretaceous sample). The uncertainties are based on the most extreme mixing curve that still fits the 95% confidence intervals on the data.

Not all the leachate data are consistent with the model mixing relationships, and in particular there are a small number of analyses that stand out as outliers. For the uncleaned samples of the Holocene carbonate, the 0.2 M acetic acid leachate is clearly one such analysis. Clarkson et al. (2020) have already noted that this leaching approach for this sample demonstrates features suggestive of incomplete carbonate dissolution. Calcium concentrations in the leachates confirm that the extent of carbonate extraction in this sample is low (Table 1), but not the lowest of all the approaches applied to uncleaned samples. Perhaps more importantly, this reagent is not buffered and, while the pH at the end of the leaching experiments was generally the same as at the start, for this experiment it was 3 log units higher. There is almost certainly potential for re-adsorption of metals on to undigested carbonate residues, and perhaps clays, possibly associated with isotope fractionation. This also appears to be the case for Mo isotopes (Clarkson et al., 2020). For the Cretaceous sample, the 7 M HCl leachates, particularly for the uncleaned fraction, represent further clear outliers on Figs. 4 and 5. Although this discrepancy does not have a clear explanation, it could be related to the different sensitivities of detrital minerals to leaching or the partial leaching of more refractory minerals. Though we see the potential for re-adsorption as potentially explaining the deviations of specific samples from the mixing relationships in Figs. 4 and 5, we also suggest that the fact that the majority of the data conform to these model mixing curves imply that re-adsorption does not have a major impact.

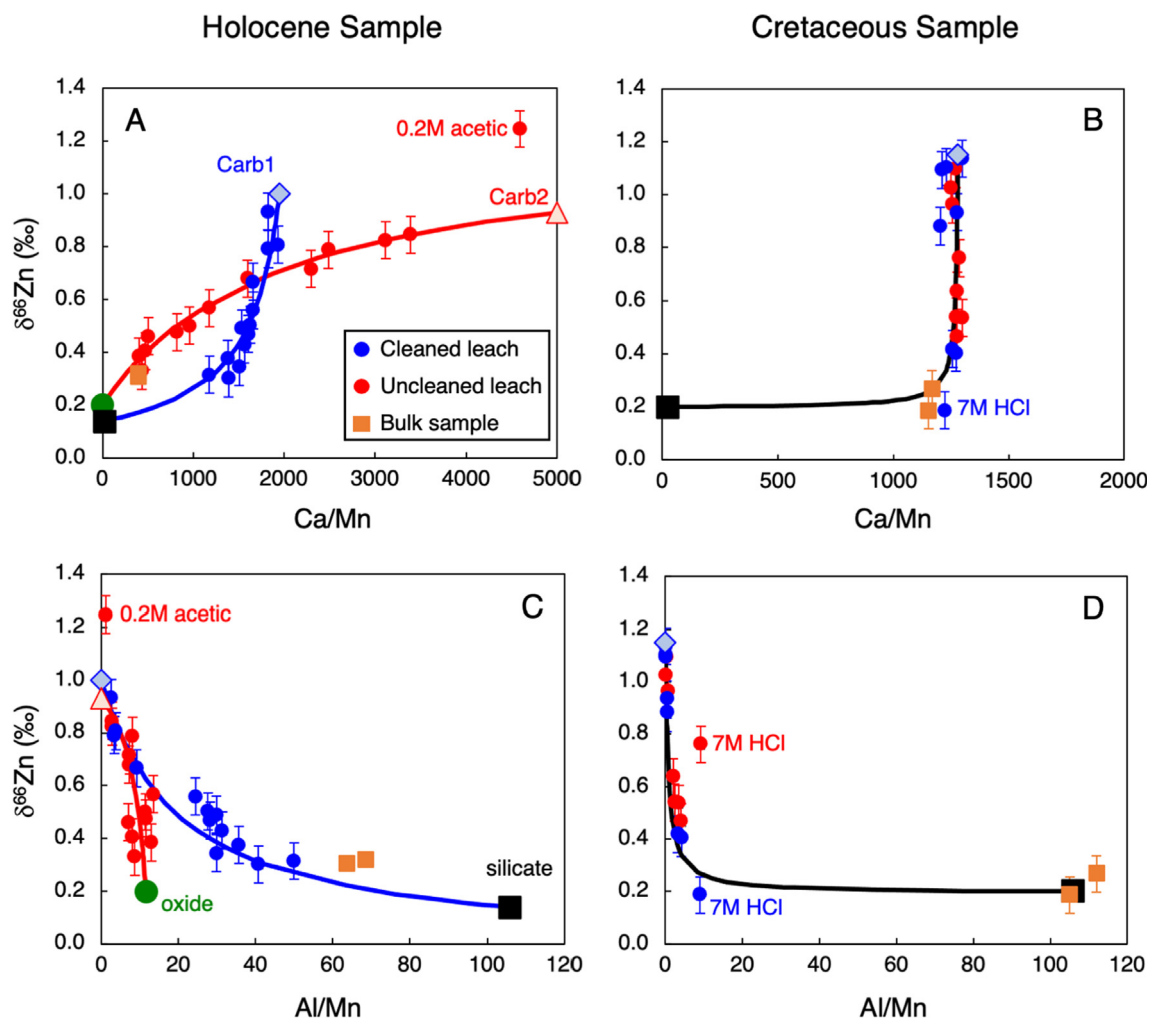


Fig. 4. Zinc isotope data and trace element ratios (molar) for the Holocene and Cretaceous sample considered in terms of mixing relationships between the end-members defined in terms of Ca/Mn and Al/Mn, and discussed in the text (see also Fig. 3). Isotope compositions of the end-members required by these data are also discussed in the text. Uncertainties on isotope data are long-term reproducibilities. The data from selected leachate experiments that do not fit these mixing curves are specifically labelled. Further details of the mixing calculations are given in the Appendix.

#### 4.3. The identity of the hypothesised pure carbonate end-members

In this section, we discuss the potential origins of the carbonate end-members, a discussion that is of importance to the meaning of their Zn isotope compositions.

The leachates of uncleaned Holocene samples form a clear array between a potential carbonate end-member, Carb2, and one that resembles an Fe-Mn oxide (Fig. 3A). Since these samples did not undergo the reductive cleaning procedure, it is possible that Carb2 itself simply represents surficial contamination. In particular, it is the weaker acid leachates (acetic acid, 0.2 M HCl) that lie beyond Carb1 in Fig. 3A, and that require the existence of this Carb2 reservoir. The fact that these leachates lie furthest from the end-member identified as an Fe-Mn oxide phase on Fig. 3A is also consistent with the previous suggestion (Poulton and Canfield, 2005) that buffered acetic acid

(pH 4–5) is thought not to attack Fe-Mn oxides. We note again the anomalous nature of the 0.2 M acetic acid leachate in many of the mixing plots on Figs. 3–5, probably, as noted in the previous section, due to incomplete digestion coupled to re-adsorption onto residual surfaces at high experimental pH (final pH 6). The other weak leachates, however, point to a Zn isotope composition for end-member Carb2 that is very similar to the other high Ca/Mn end-member, denoted Carb1 on the mixing plots (Fig. 4). This consistency between the Zn isotope compositions of the two high Ca/Mn end-members seems to argue against the suggestion that Carb2 represents surface contamination. This consistency could, though, also be explained by re-precipitation of some carbonate dissolved during the cleaning process.

One obvious explanation of the two apparent carbonate end-members in the Holocene sample is simply that different carbonate phases with different Mn contents are being

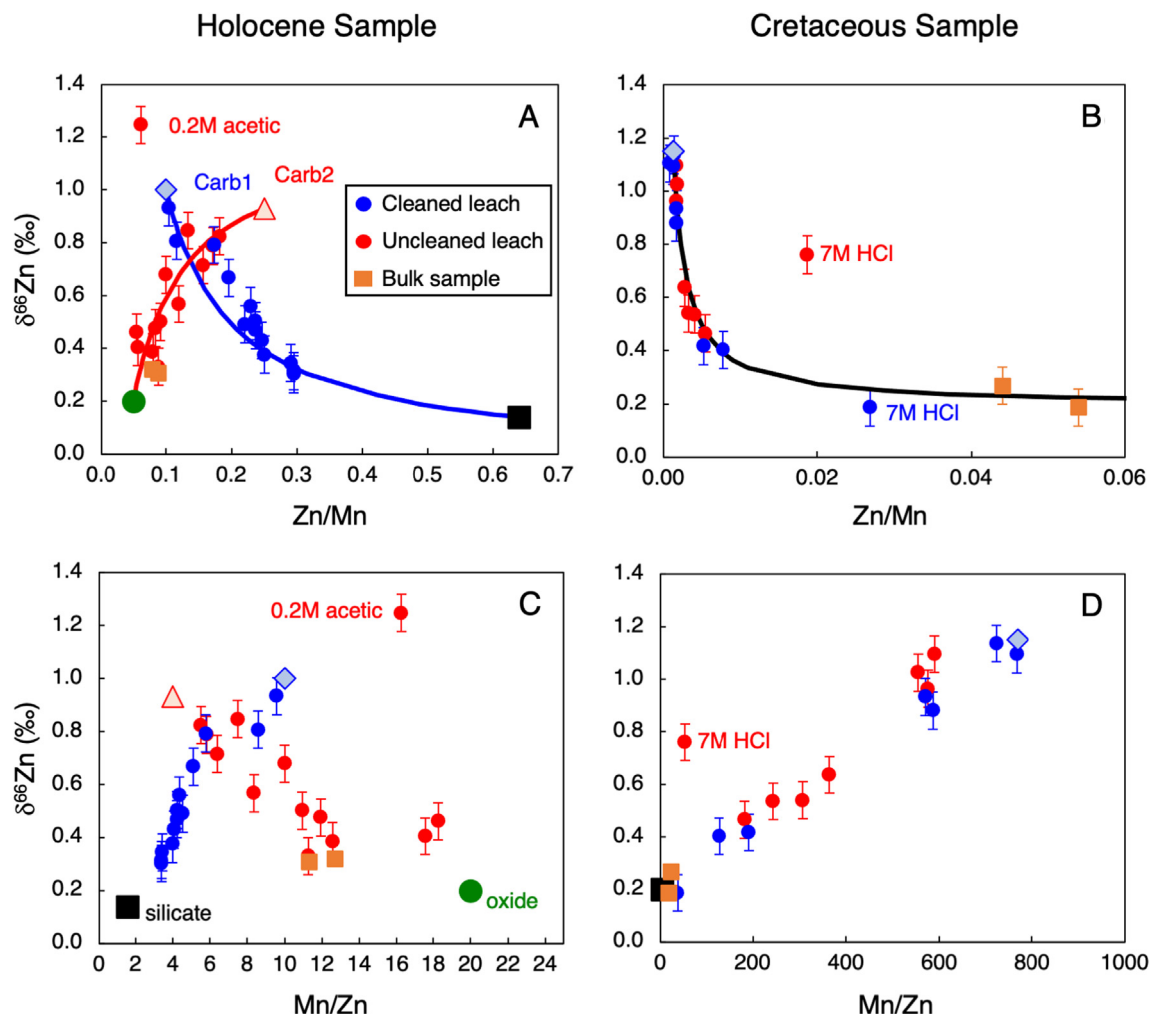


Fig. 5. Zinc isotope data and molar Zn/Mn ratios for the Holocene and Cretaceous samples are considered in terms of mixing relationships between the end-members defined by Fig. 3. Uncertainties on isotope data are long-term reproducibilities. The data from selected leachate experiments that do not fit these mixing curves are specifically labelled. Further details of the mixing calculations are given in the Appendix.

leached in the experiments with cleaned versus uncleaned samples. It is clear from Fig. 1 that a significant portion (25–45%) of the initial carbonate in the bulk sample is dissolved and lost during the cleaning process. It is possible that the phase represented by end-member Carb2 is dissolved by reductive cleaning, so that its impact is only seen in uncleaned samples, whereas the leachates of cleaned samples are dominated by a carbonate phase that survives the cleaning process – Carb1. It is noteworthy that the main difference in the chemistry between the two putative carbonate phases are that Carb1 has a Mn/Ca ratio around 500  $\mu\text{mol/mol}$ , whereas that of Carb2 is lower at about 200  $\mu\text{mol/mol}$ . Though Pena et al. (2005) suggest that Mn-Mg-rich carbonates coating the inner surfaces of foraminifera are removed by reductive cleaning, Boyle (1983) suggests the opposite. Further, a study of planktonic foraminifera from this specific sample (Burton and Vance, 2000) observed elevated Mn/Ca even after reductive cleaning, suggesting that some Mn-rich carbonate coatings remain. The data presented here are consistent with a high

Mn/Ca phase surviving the cleaning process, remaining to contribute to Carb1, while other components are dissolved. In this view, Carb2 could represent a fine-grained carbonate, such as a cement, that is prone to dissolution during reductive cleaning.

In contrast to the Holocene carbonate sample, there appears to be only one carbonate end-member in the Cretaceous sample (Figs. 4 and 5). Clarkson et al. (2020) suggest that there are no Fe-Mn oxide coatings in this sample and, compared to the Holocene sample, the Cretaceous sample contains higher Mn concentrations. Both these observations are consistent with a reducing setting for this sample, beneath the sediment-water interface (e.g. Shimmiel and Price, 1986; Calvert and Pedersen, 1993), where Mn oxides will be unstable and where Mn carbonate has been suggested to be the important solid Mn phase. This sample also has distinctly lower contents of Zn and other trace metals than the Holocene sample. Although speculative, it seems that trace metal abundances in this sample are impacted by associated processes, i.e. re-precipitation with Ca-Mn

carbonate cements and/or release to pore waters and to the water column (Clarkson et al., 2020). The conclusions of Clarkson et al. (2020), are very similar to those arrived at here: U/Ca shows a consistent decrease with reductive cleaning across all leaching reagents, suggesting the removal of a second carbonate phase.

We stress that further work is required to identify the specific nature of the different pure carbonate end-members in these and other samples. What is most important for this study is that, for example, both carbonate end-members in the Holocene sample have the same  $\delta^{66}\text{Zn}$ . This is not entirely expected – given that the carbonate in these samples is made up of both primary biogenic and secondary authigenic phases, not all of which are expected to be simply related or to have the same Zn isotope composition. The meaning of that isotope composition, and its relationship to the contemporary ocean, is discussed in the next section.

#### 4.4. Zn isotope composition of carbonate end-members and relationship to contemporary seawater

The modern global deep ocean (below 500 m depth), which is quantitatively representative of the oceanic dissolved Zn pool, exhibits a notably homogeneous  $\delta^{66}\text{Zn}$  signature at  $+0.46 \pm 0.08\text{‰}$  (Fig. 2 and references therein), while surface water has been observed to be much more variable, and predominantly isotopically lighter ( $\delta^{66}\text{Zn}$  down to  $-1.1\text{‰}$ ; Conway and John, 2014; John et al., 2018; Lemaitre et al., 2020), particularly in the Atlantic. The light isotope composition of the modern upper Atlantic Ocean was originally interpreted as reflecting preferential removal of the heavy isotope by scavenging (Conway and John, 2014). However, Lemaitre et al. (2020) used mixing relationships to demonstrate that isotopically light Zn in the North Atlantic is associated with Zn addition, not removal, and that the un-contaminated upper ocean  $\delta^{66}\text{Zn}$  is the same as the deep ocean, at around  $+0.5\text{‰}$ . This signature of Zn addition coupled to light isotopes is also absent in the surface waters of the Southern Ocean, remote from the sources of anthropogenic contamination. This geographic pattern for Zn is very similar to that for Pb isotopes, well-known to be anthropogenically-contaminated in the modern ocean (Boyle et al., 2014).

The above suggestion receives support from another recent study. Little et al. (2021) find that cold-water corals collected beneath 500 m generally record a  $\delta^{66}\text{Zn}$  that is close to the deep ocean. They also suggest that the fact that samples collected in the upper 300 m are different from locally light seawater, and shifted towards the deep-ocean value, is due to the fact that corals are integrating Zn over a century, lending support to the suggestion that the upper ocean is anthropogenically-disturbed for Zn isotopes. So, we focus here on the suggestion that the pre-anthropogenic whole ocean has a single  $\delta^{66}\text{Zn}$  of  $+0.46 \pm 0.08\text{‰}$  (see caption to Fig. 2), though we acknowledge that a definitive proof that the upper ocean is pervasively anthropogenically-contaminated requires further work. Thus, the two carbonate end-members for the modern deep ocean sample studied here display  $\delta^{66}\text{Zn}$  values at  $+0.93 \pm$

$0.10\text{‰}$  and  $+0.90 \pm 0.10\text{‰}$  (Figs. 4 and 5), fractionated by  $0.4\text{--}0.5\text{‰}$  from seawater. We note that this approach is different from that recently taken in Zhao et al. (2021), where carbonate  $\delta^{66}\text{Zn}$  are directly compared to local modern, we suggest anthropogenically-contaminated, surface seawater.

Dong and Wasylenki (2016) conducted experiments to determine the Zn isotope fractionation upon sorption to inorganic calcite surfaces, and reported a  $\Delta^{66}\text{Zn}_{\text{adsorbed-solution}}$  of  $+0.41 \pm 0.18\text{‰}$  and  $+0.73 \pm 0.08\text{‰}$  in low and high ionic strength systems, respectively. Synthetic seawater was used for the high ionic strength experiment, and thus the associated fractionation value,  $+0.73\text{‰}$  would be applicable to our carbonate endmember compositions if sorption was the main control on incorporation. On the other hand, a recent co-precipitation experiment for Zn and inorganic calcite found a constant  $\Delta^{66}\text{Zn}_{\text{calcite-aqueous Zn}^{2+}}$  of  $+0.58 \pm 0.05\text{‰}$  (Mavromatis et al., 2019), independent of pH. This can be used, in conjunction with the  $\delta^{66}\text{Zn}$  of Carb1 and Carb2 in the Holocene sample, to predict a  $\delta^{66}\text{Zn}$  of the  $\text{Zn}^{2+}$  pool in contemporary seawater of  $+0.35$  and  $+0.42\text{‰}$  (Fig. 6). Though these values overlap with the modern deep ocean total dissolved pool, given the uncertainties (Fig. 6), the fact that they lie at the lower end of the deep ocean range is consistent with the nature of Zn speciation in real seawater versus the experiments. A large fraction of the dissolved pool of Zn in the oceans is organically-complexed, and experiments have shown that free  $\text{Zn}^{2+}$  will have a  $\delta^{66}\text{Zn}$  that is somewhere between 0 and  $0.2\text{‰}$  lighter than the dominant pool of organically-complexed Zn (see review in Moynier, et al. 2017).

#### 4.5. Comparison with previous data: variable Zn isotope fractionations from seawater into carbonate

Previous studies of bulk carbonate sediment  $\delta^{66}\text{Zn}$  applied to geological history have often focused on

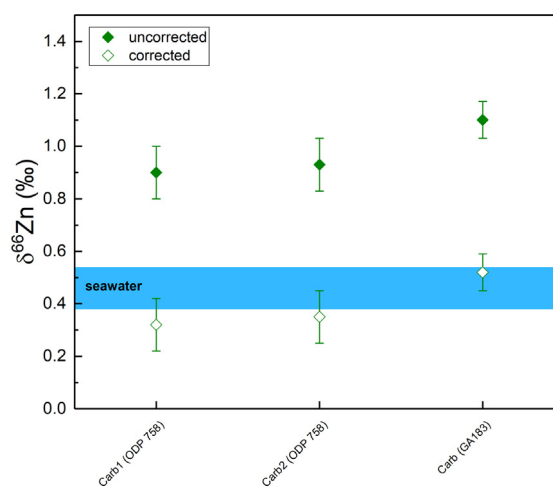


Fig. 6. The  $\delta^{66}\text{Zn}$  isotope compositions of the different carbonate end-members extracted from the Holocene (ODP 758) and the Cretaceous samples (GA183) (filled green diamonds), and those inferred for contemporary seawater through correction for the isotope fractionation obtained experimentally (Mavromatis et al., 2019). The blue shaded bar indicates the  $\delta^{66}\text{Zn}$  for the modern deep ocean.

excursions associated with periods of extreme environmental perturbations (Kunzmann et al., 2013; John et al., 2017; Liu et al., 2017; Sweere et al., 2018; Chen et al., 2021). All of these studies used unbuffered acetic acid of various strengths, sometimes with heating, to selectively digest carbonate. Given our results here that demonstrate greater silicate contributions in even weak mineral acids, more so with longer acid exposure time, we would expect heating to further mobilize Zn from contaminants. In our study, unbuffered 1 M acetic acid accesses Zn that is up to 0.3‰ lower than pure carbonate end-members, due to contamination with either silicate or Fe-Mn oxide (Tables 1, 2). The current investigation suggests that buffering the leaching acid yields a result that overlaps with the pure carbonate end-members. On the other hand, at least for the two samples studied here and given care with the choice of leaching reagent, it is not obvious that samples need to be reductively cleaned to obtain a pure carbonate end-member  $\delta^{66}\text{Zn}$ . Druce et al. (2022) reached a similar conclusion, confirming that reductive-oxidative chemical cleaning protocols are not mandatory in all cases to obtain accurate Zn isotope data, and may even be the cause of anomalous isotope effects. Nevertheless, they stress the necessity of including a reductive step to ensure removal of secondary Fe-Mn oxide coatings, but recommend omitting the use of hydrazine due to its potential interference with the citrate chemistry.

Despite the above methodological uncertainty, away from the excursions that were the main target of the earlier studies, what is remarkable is how little carbonate  $\delta^{66}\text{Zn}$  varies from that obtained here for the Holocene sample. Thus, for example, the late Ediacaran carbonates from the interval furthest removed from the Snowball Earth period, and therefore likely representing a recovered state of the oceans, have  $\delta^{66}\text{Zn} = +0.87\text{‰}$  (Kunzmann et al., 2013; John et al., 2017). Liu et al. (2017) document a dramatic excursion to very low values in carbonate  $\delta^{66}\text{Zn}$  just before the Permo-Triassic Boundary, but the background values away from this excursion are around  $+1 \pm 0.2\text{‰}$ . Above and below OAE2, stratigraphically well above and below prominent excursions associated with the anoxic event itself and the Plenus Cold Event that interrupts it, carbonate  $\delta^{66}\text{Zn}$  are mostly around  $+1.1\text{‰}$  (Sweere et al., 2018; Chen et al., 2021). The Cretaceous sample studied in detail here comes from the same section as studied in Chen et al. (2021) and the carbonate end-member yields a  $\delta^{66}\text{Zn}$  of  $+1.10\text{‰}$ .

These values for background  $\delta^{66}\text{Zn}$  in carbonate are all rather similar to each other, and are all similarly heavier than modern seawater – the reservoir that the Zn in at least the Holocene sample studied here must be derived. The Mavromatis et al. (2019) experimental study cited earlier found a  $\Delta^{66}\text{Zn}_{\text{calcite-aqueous Zn}^{2+}} = +0.58 \pm 0.05\text{‰}$ . In the context of these experiments, all the data for modern and ancient carbonates appear to imply a  $\text{Zn}^{2+}$  pool of seawater that might have varied between  $+0.3$  and  $+0.6\text{‰}$ , similar to the modern deep ocean. The leaching of bulk sediment almost certainly accesses authigenic cements that are probably precipitated inorganically, at close to equilibrium with bottom water (e.g. Milliman, 1974; Carpenter et al., 1991;

Noé et al., 2006), in a pseudo-open system. If the interpretation of the experimental results in Mavromatis et al. (2019) is correct, then this variability in background  $\delta^{66}\text{Zn}$ , outside environmental perturbations, may have as much to do with changes in speciation as changes in the Zn isotope composition of the total dissolved pool of Zn, not just pH-dependent but also associated with changes in the extent of organic speciation (c.f. Little et al., 2021; Druce et al., 2022).

In complete contrast to all of this, the recent results for cold-water corals presented in Little et al. (2021) incorporate Zn that is isotopically very close to the water they are found in, with a  $\Delta_{\text{coral-seawater}}$  averaging  $+0.03\text{‰}$  (Little et al., 2021). The first published zinc isotope measurement of hand-picked benthic foraminifera reports a  $\Delta_{\text{foraminifera-seawater}}$  of  $0.08 \pm 0.08\text{‰}$  (Druce et al., 2022), lending further support to the assumption that Zn isotopes are not fractionated upon incorporation into biogenic carbonate. Potential reasons for this contrast with the experimental results are discussed extensively in Little et al. (2021), and remain unclear. But it may be related to the fact that biogenic calcite incorporates the  $\text{Zn}^{2+}$  species (van Dijk et al., 2017), and that it is precipitated from a calcifying fluid that is ultimately derived from seawater, and in a semi-closed system with quantitative extraction of the Zn pool (e.g. Elderfield et al., 1996; Adkins et al., 2003). Data from a further very recent study of Zn isotope incorporation into carbonate (Zhao et al., 2021) are more difficult to interpret in this context. First, Zhao et al. (2021) extracted Zn from uncleaned carbonate using unbuffered 2 M acetic acid with heating, a method that is likely to be compromised by contributions from Fe-Mn coatings and detrital silicates. Unfortunately, no trace element data (e.g. Mn) are available to assess this potential issue (Zhao et al., 2021). Second, given that the upper ocean is likely to be anthropogenically contaminated for Zn, and as noted in Little et al. (2021), the Zn isotope composition of the reservoir from which un-dated shallow water carbonate is derived is unclear. Nonetheless, and excluding one extremely light value, the carbonates reported in Zhao et al. (2021) vary between local present-day seawater and a value about 0.6‰ heavier than the deep ocean value, consistent with the variability seen in Little et al. (2021) and in this study.

Thus, there have now been four studies that compare modern carbonate with modern seawater (this study, Little et al., 2021; Zhao et al., 2021; Druce et al., 2022). This small number of studies have uncovered a  $\Delta^{66}\text{Zn}_{\text{calcite-seawater}}$  that varies by at least 0.6‰ (Fig. 7). Clearly, the variability between modes of incorporation of Zn into carbonate suggest that caution must be exercised in interpreting Zn isotope variations in carbonate solely in terms of the oceanic isotope composition, and dramatic changes in the isotopic mass balance of seawater, its inputs and outputs. This is particularly the case during periods of extreme environmental perturbation that must profoundly alter the physical and chemical controls on Zn speciation in seawater as well as its incorporation into carbonate. It is, however, interesting that, in the case of OAE2 (Sweere et al., 2018), similar  $\delta^{66}\text{Zn}$  trends are found in different

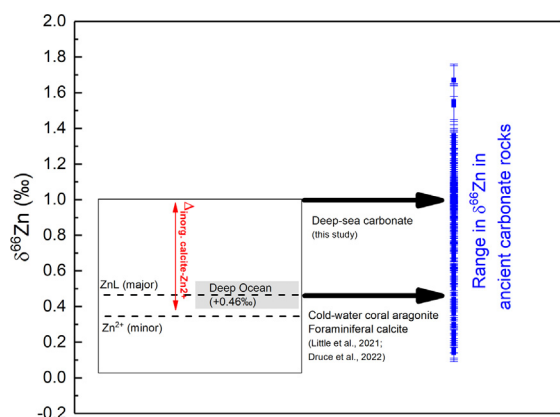


Fig. 7. The  $\delta^{66}\text{Zn}$  values on the right (blue symbols) illustrate the wide range of isotopic compositions measured in several studies of ancient carbonates (John et al., 2017; Sweere et al., 2018; Chen et al., 2021; this study). The red double arrow indicates the experimentally determined fractionation between the aqueous  $\text{Zn}^{2+}$  species and the Zn isotopic composition of inorganic calcite (Mavromatis et al., 2019). This fractionation is very close to the difference between  $\delta^{66}\text{Zn}$  in deep-sea carbonates (this study) and the average  $\delta^{66}\text{Zn}$  of the oceanic total dissolved pool, which in turn is recorded in cold-water coral aragonite and foraminiferal calcite without fractionation (Little et al., 2021; Druce et al., 2022). This fractionation discrepancy between different types of carbonates could explain a lot of the variability seen in the  $\delta^{66}\text{Zn}$  carbonate record.

sections with different depositional settings, depths and carbonate mineralogies. This suggests there is some potential for perturbations in the global Zn cycle to be recorded in carbonates, even if the precise relationship to seawater is unclear.

## 5. SUMMARY AND CONCLUDING REMARKS

Our detailed investigation of the application of reductive cleaning, different leaching acids and acid strengths to bulk marine sediment sheds new light on the Zn reservoirs in these samples, how contaminant phases can compromise the extraction of the Zn content and isotope composition of carbonate end-members. Our results suggest that the use of buffered 1 M acetic acid is required to avoid influences from contaminant phases present in the bulk sample, and to ensure complete dissolution of the carbonate phase. Analysis of trace element and isotope data in terms of mixing between carbonate components and contaminants has revealed the presence in these samples of multiple end-members, whose chemical and isotope characteristics are clearly identified.

Carbonate  $\delta^{66}\text{Zn}$  from bulk sediment leachates seem to reflect the isotopic composition of the  $\text{Zn}^{2+}$  pool of the deep ocean (which will be at the lower end of the range measured for the total dissolved pool) when corrected by the isotopic fractionation determined for  $\Delta^{66}\text{Zn}_{\text{calcite-aqueous Zn}^{2+}}$  in inorganic calcite coprecipitation experiments (Mavromatis et al., 2019). In contrast, biogenic carbonates (deep-sea corals, foraminiferal calcite) appear to directly record seawater  $\delta^{66}\text{Zn}$  without

significant fractionation (Little et al., 2021; Druce et al., 2022). Thus, at least two different fractionation behaviours exist for Zn in carbonates, and there appears to be little contribution from an unfractionated component in these deep-sea bulk samples.

These conclusions have important consequences for the interpretation of published Zn isotope data, using a similar approach to that used here to extract the carbonate signature, across periods of environmental change in the geological record (e.g. Kunzmann et al., 2013; John et al., 2017; Liu et al., 2017; Sweere et al., 2018; Chen et al., 2021). For example, given the fact that the carbonate signatures extracted here are consistent with the experiments of Mavromatis et al. (2019) and what we know about speciation and isotope composition in the modern ocean, published Zn isotope records point to a rather invariant situation in the ocean in the past. Interpretation of short-lived but prominent excursions to much lighter isotope compositions in published records in terms of the same framework would require an oceanic  $\text{Zn}^{2+}$  pool that seems implausibly light (as light as 0.2‰, e.g. Liu et al., 2017; Chen et al., 2021). We suggest that these excursions may relate as much to differences in the nature of Zn isotope incorporation into carbonate as excursions in dissolved seawater Zn isotopes.

Future palaeoceanographic studies analysing Zn isotopes in the marine carbonate record should consider these different pathways of carbonate precipitation and associated Zn fractionation constraints.

## Declaration of Competing Interest

The authors declare that they have no known competing financial interests or personal relationships that could have appeared to influence the work reported in this paper.

## ACKNOWLEDGMENTS

We would like to thank Susan H. Little and Tim C. Sweere for their helpful comments on the manuscript, and Corey Archer for valuable laboratory assistance. This research was funded by the Swiss National Science Foundation (grants 200020\_165904 and 200021-184873) and the European Union's Horizon 2020 research and innovation programme under the Marie Skłodowska-Curie grant agreement No 795722. We thank the Associate Editor Weiqiang Li, Bleuenn Guéguen, Patrick Blaser and two anonymous reviewers for comments that helped us to significantly improve the manuscript.

## APPENDIX – MIXING CALCULATIONS

This appendix details the mixing calculations illustrated in Figs. 3–5 of the main paper. Our main objective is to investigate the degree to which such calculations can constrain the Zn isotope composition of the carbonate end-members and, in particular, to use these constraints to identify the best leaching approach to extract this Zn isotope composition. In addition, we seek to better understand the nature of the putative silicate and Fe-Mn oxide contaminants contributing to the leachates.

Element ratios for the mixing curves in Figs. 4 and 5 were calculated (e.g. Albarède, 2010) as follows:

$$\left(\frac{X}{Y}\right)_{\text{mix}} = \left(\frac{X}{Y}\right)_{\text{em1}} + \left(\left(\frac{X}{Y}\right)_{\text{em2}} - \left(\frac{X}{Y}\right)_{\text{em1}}\right) \left(\frac{f_{\text{em2}}[Y]_{\text{em2}}}{[Y]_{\text{mix}}}\right) \quad [1]$$

where  $\left(\frac{X}{Y}\right)_{\text{mix},\text{em1},\text{em2}}$  is the ratio of the abundance of element X to element Y in the mixture, end-member 1, end-member 2 (e.g. silicate, oxide, carbonate),  $f_{\text{em1},2}$  is the fraction of end-member 1 or 2 in the mixture and  $[Y]_{\text{mix}}$  is the concentration of element Y in the mixture:

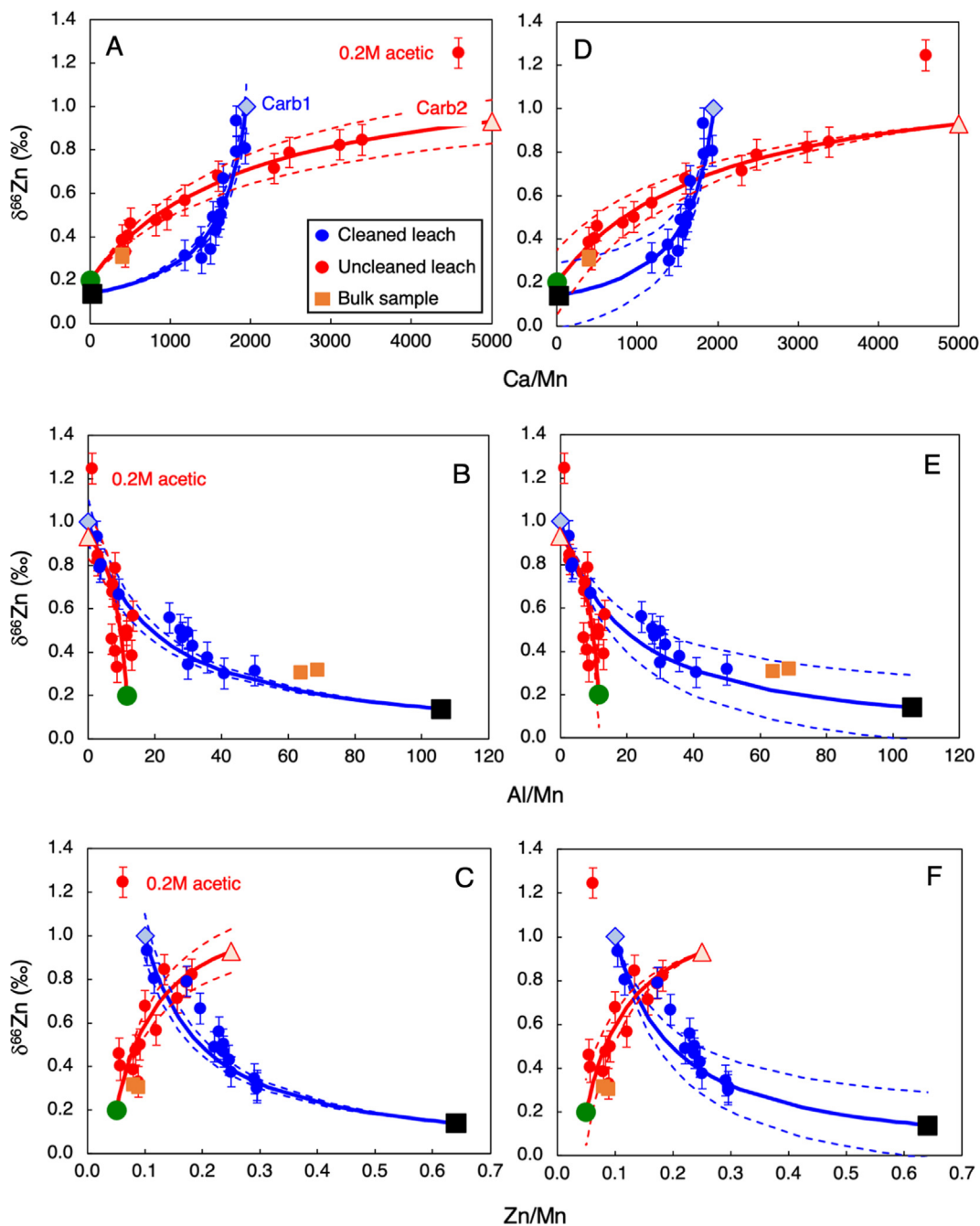


Fig. A1. Leaching data for the Holocene sample (elemental ratios are molar) with best-fit model mixing curves (solid lines) between an Fe-Mn oxide (filled green circles) and a carbonate end-member (Carb2, red triangle) for the uncleaned samples, and between a silicate (filled black square) and a second carbonate end-member (Carb1, blue diamond) for cleaned samples. The dashed lines in panels A-C show the mixing curves for  $\delta^{66}\text{Zn}$  of model carbonate end-members  $\pm 0.1\text{‰}$  from the best fit value. The dashed lines in panels D-F show the mixing curves for  $\delta^{66}\text{Zn}$  of contaminant silicate or Fe-Mn oxide end-members  $\pm 0.15\text{‰}$  from the best fit value.



$$[Y]_{\text{mix}} = f_{em1}[Y]_{em1} + f_{em2}[Y]_{em2} \quad [2]$$

Zinc isotope compositions for the mixing curves in Figs. 4 and 5 were calculated as follows:

$$(\delta^{66}\text{Zn})_{\text{mix}} = (\delta^{66}\text{Zn})_{em1} f_{em1} \frac{[\text{Zn}]_{em1}}{[\text{Zn}]_{\text{mix}}} + (\delta^{66}\text{Zn})_{em2} f_{em2} \frac{[\text{Zn}]_{em2}}{[\text{Zn}]_{\text{mix}}} \quad [3]$$

where  $[\text{Zn}]_{\text{mix}}$ ,  $em1$ ,  $em2$  are the concentrations of Zn in the mixture (calculated as for equation [2]), and in end-members 1 and 2.

The starting point for our exploration of the relevant end-members in the bulk carbonate sediment of the Holocene sample is the elemental ratios (Fig. 3). The linear least-squares fit to the pre-cleaned samples clearly defines an array in Ca/Mn versus Al/Mn space, between an end-member with high Ca/Mn (Carb1 on Fig. 3A) and a second end-member with high Al/Mn and a Ca/Mn near zero. The chemistry of this latter end-member is very close to the suspended loads of large rivers (Viers et al., 2009), and is likely silicate/clays. The least-squares linear fit to the data for samples that had not been pre-cleaned (excluding the 0.2 M acetic acid analysis for the reasons discussed in the main text) suggests mixing between a second carbonate end-member (Carb2 on Fig. 3A) and an end-member with a low Ca/Mn and Al/Mn, identical in chemistry to that of Fe-Mn oxide coatings on cold water corals (Little et al., 2021). The Ca/Mn ratios, at Al/Mn = 0, of the carbonate end-members are used to locate their positions in subsequent diagrams.

The Zn/Mn ratios of the end-members are defined by the intersection of least-squares linear fits to the two data arrays in Ca/Mn versus Zn/Mn space (Fig. 3B, again omitting the 0.2 M acetic acid leachate), with the Ca/Mn ratio for these end-members as defined by Fig. 3A. The Zn/Mn ratio obtained for the Fe-Mn oxide contaminant is again identical to that for Fe-Mn oxide coatings on cold water corals (Little et al., 2021). However, the data array for the cleaned samples requires a silicate end-member that has a Zn/Mn ratio that is a factor of four higher than that reported for the suspended loads of large rivers in Viers et al. (2009).

The mixing calculations involving isotope ratios require end-member elemental ratios, obtained as outlined above, as well as concentrations and isotope compositions. The concentrations for the silicate and oxide members were obtained from the concentrations reported in Viers et al. (2009) for the silicate end-member and in Manheim and Lane-Bostwick (1991) for the Fe-Mn oxide end-member, but with the adjustment to the Zn concentration of the silicate end-member to take account of the higher Zn/Mn mentioned above. Carbonate concentrations are calculated from end-member element/Ca ratios, assuming stoichiometric  $\text{CaCO}_3$ . Then, the isotope compositions of the end-members were adjusted to obtain the best least-squares fit to the data arrays in Figs. 4 and 5 of the main paper.

The degree to which these mixing calculations constrain end-member carbonate Zn isotope compositions is illustrated in Fig. A1. Panels A-C show the mixing arrays for

the best-fit carbonate  $\delta^{66}\text{Zn}$  (A-C, solid lines) and for 0.1‰ either side of this (dashed lines). Panels D-F show the mixing arrays for the best-fit contaminant  $\delta^{66}\text{Zn}$  (D-F, solid lines) and for 0.15‰ either side of this (dashed lines). The Ca/Mn versus  $\delta^{66}\text{Zn}$  data (A, D) show the least scatter, and this plot provides a good constraint on the Zn isotope composition of Carb2 at  $+0.93 \pm 0.10$ , and the Fe-Mn oxide contaminant, at  $+0.20 \pm 0.15$ ‰. This  $\delta^{66}\text{Zn}$  is within uncertainty of that obtained via leaching of the bulk sample with buffered acetic acid of both cleaned and uncleaned samples (0.79–0.85‰). The constraint on the  $\delta^{66}\text{Zn}$  of Carb2 is looser, but we note that the best-fit value also overlaps within analytical uncertainty both with that of Carb1 and with the buffered acetic acid leachates. This latter conclusion also applies to the data for the Cretaceous sample, to which we applied the same approach, though here the highly curved mixing arrays yield imprecise constraints on the carbonate end-member.

## APPENDIX A. SUPPLEMENTARY DATA

Supplementary data to this article can be found online at <https://doi.org/10.1016/j.gca.2022.02.029>.

## REFERENCES

- Adkins J. F., Boyle E. A., Curry W. B. and Lutringer A. (2003) Stable isotopes in deep sea corals and a new mechanism for “vital effects”. *Geochim. Cosmochim. Acta* **67**, 1129–1143.
- Albarède F. (2010) *Introduction to Geochemical Modelling*. Cambridge Univ. Press, Cambridge.
- Andersen M. B., Stirling C. H. and Weyer S. (2017) Uranium isotope fractionation. *Rev. Mineral. Geochem.* **82**, 799–850.
- Archer C. and Vance D. (2004) Mass discrimination correction in multiple-collector plasma source mass spectrometry: an example using Cu and Zn isotopes. *J. Anal. At. Spectrom.* **19**, 656.
- Archer C., Andersen M. B., Cloquet C., Conway T. M., Dong S., Ellwood M., Moore R., Nelson J., Rehkämper M., Rouxel O., Samanta M., Shin K.-C., Sohrin Y., Takano S. and Wasylenko L. (2017) Inter-calibration of a proposed new primary reference standard AA-ETH Zn for zinc isotopic analysis. *J. Anal. At. Spectrom.* **32**, 415–419.
- Barker S., Cacho I., Benway H. and Tachikawa K. (2005) Planktonic foraminiferal Mg/Ca as a proxy for past oceanic temperatures: a methodological overview and data compilation for the Last Glacial Maximum. *Quat. Sci. Rev.* **24**, 821–834.
- Bermin J., Vance D., Archer C. and Statham P. J. (2006) The determination of the isotopic composition of Cu and Zn in seawater. *Chem. Geol.* **226**, 280–297.
- Bomou B., Adatte T., Tantawy A. A., Mort H., Fleitmann D., Huang Y. J. and Föllmi K. B. (2013) The expression of the Cenomanian-Turonian oceanic anoxic event in Tibet. *Palaeogeogr. Palaeoclimatol. Palaeoecol.* **369**, 466–481.
- Boyle E. A. (1981) Cadmium, zinc, copper, and barium in foraminifera tests. *Earth Planet. Sci. Lett.* **53**, 11–35.
- Boyle E. A. (1983) Manganese carbonate overgrowths on foraminifera tests. *Geochim. Cosmochim. Acta* **47**, 1815–1819.
- Boyle E. A. and Keigwin L. D. (1985) Comparison of Atlantic and Pacific paleochemical records for the last 215,000 years: changes in deep ocean circulation and chemical inventories. *Earth Planet. Sci. Lett.* **76**, 135–150.
- Boyle E. A., John S., Abouchami W., Adkins J. F., Echegoyen-Sanz Y., Ellwood M., Flegel A. R., Fornace K., Gallon C.,

- Galer O., Gault-Ringold M., Lacan F., Radic A., Rehkamper M., Rouxel O., Sohrin Y., Stirling C., Thompson C., Vance D., Xue Z. and Zhao Y. (2012) GEOTRACES IC1 (BATS) contamination-prone trace element isotopes Cd, Fe, Pb, Zn, Cu, and Mo intercalibration. *Limnol. Oceanogr. – Meth.* **10**, 653–665.
- Boyle E. A., Lee J.-M., Echegoyen Y., Noble A., Moos S., Carrasco G., Zhao N., Kayser R., Zhang J., Gamo T., Obata H. and Norisuye K. (2014) Anthropogenic lead emissions in the ocean: the evolving global experiment. *Oceanography* **27**, 69–75.
- Brennecke G. A., Herrmann A. D., Algeo T. J. and Anbar A. D. (2011) Rapid expansion of oceanic anoxia immediately before the end-Permian mass extinction. *Proc. Natl. Acad. Sci. U.S.A.* **108**, 17631–17634.
- Bruland K. W., Orians K. J. and Cowen J. P. (1980) Reactive trace metals in the stratified central North Pacific. *Geochim. Cosmochim. Acta* **58**, 3171–3182.
- Burton K. W. and Vance D. (2000) Glacial–interglacial variations in the neodymium isotope composition of seawater in the Bay of Bengal recorded by planktonic foraminifera. *Earth Planet. Sci. Lett.* **176**, 425–441.
- Calvert S. E. and Pedersen T. F. (1993) Geochemistry of recent oxic and anoxic marine sediments: implications for the geological record. *Mar. Geol.* **113**, 67–88.
- Carpenter S. J., Lohmann K. C., Holden P., Walter L. M., Huston T. J. and Halliday A. N. (1991)  $\delta^{18}\text{O}$  values,  $^{87}\text{Sr}/^{86}\text{Sr}$  and Sr/Mg ratios of Late Devonian abiogenic marine calcite: implications for the composition of ancient seawater. *Geochim. Cosmochim. Acta* **55**, 1991–2010.
- Chen X., Sageman B. B., Yao H., Liu S., Han K., Zou Y. and Wang C. (2021) Zinc isotope evidence for paleoenvironmental changes during Cretaceous Oceanic Anoxic Event 2. *Geology* **49**, 412–416.
- Clarkson M. O., Stirling C. H., Jenkyns H. C., Dickson A. J., Porcelli D., Moy C. M., Pogge von Strandmann P. A. E., Cooke I. R. and Lenton T. M. (2018) Uranium isotope evidence for two episodes of deoxygenation during Oceanic Anoxic Event 2. *Proc. Natl. Acad. Sci. U.S.A.* **115**, 2918–2923.
- Clarkson M. O., Müsing K., Andersen M. B. and Vance D. (2020) Examining pelagic carbonate-rich sediments as an archive for authigenic uranium and molybdenum isotopes using reductive cleaning and leaching experiments. *Chem. Geol.* **539** 119412.
- Conway T. M. and John S. G. (2014) The biogeochemical cycling of zinc and zinc isotopes in the North Atlantic Ocean. *Global Biogeochem. Cycles* **28**, 1111–1128.
- Conway T. M. and John S. G. (2015) Cycling of iron, zinc and cadmium in the North East Pacific Ocean – insights from stable isotopes. *Geochim. Cosmochim. Acta* **164**, 262–283.
- Curry W. B., Duplessy J.-C., Labeyrie L. D. and Shackleton N. J. (1988) Changes in the distribution of  $\delta^{13}\text{C}$  of deep water  $\Sigma\text{CO}_2$  between the Last Glaciation and the Holocene. *Paleoceanogr. Paleoclimatol.* **3**, 317–342.
- Dong S. and Wasylenki L. E. (2016) Zinc isotope fractionation during adsorption to calcite at high and low ionic strength. *Chem. Geol.* **447**, 70–78.
- Druce M., Stirling C. H., Bostock H. C. and Rolison J. M. (2022) Examining the effects of chemical cleaning, leaching, and partial dissolution on zinc and cadmium isotope fractionation in marine carbonates. *Chem. Geol.* **592** 120738.
- Elderfield H., Bertram C. J. and Erez J. (1996) A biomineralization model for the incorporation of trace elements into foraminiferal calcium carbonate. *Earth Planet. Sci. Lett.* **142**, 409–423.
- Isson T. T., Love G. D., Dupont C. L., Reinhard C. T., Zumberge A. J., Asael D., Gueguen B., McCrow J., Gill B. C., Owens J., Rainbird R. H., Rooney A. D., Zhao M.-Y., Stueeken E. E., Konhauser K. O., John S. G., Lyons T. W. and Planavsky N. J. (2018) Tracking the rise of eukaryotes to ecological dominance with zinc isotopes. *Geobiology* **16**, 341–352.
- John S. G. and Conway T. M. (2014) A role for scavenging in the marine biogeochemical cycling of zinc and zinc isotopes. *Earth Planet. Sci. Lett.* **394**, 159–167.
- John S. G., Kunzmann M., Townsend E. J. and Rosenberg A. D. (2017) Zinc and cadmium stable isotopes in the geological record: a case study from the post-snowball Earth Nuccaleena cap dolostone. *Palaeogeogr. Palaeoclimatol. Palaeoecol.* **466**, 202–208.
- John S. G., Helgoe J. and Townsend E. (2018) Biogeochemical cycling of Zn and Cd and their stable isotopes in the Eastern Tropical South Pacific. *Mar. Chem.* **201**, 66–76.
- Kendall B., Dahl T. W. and Anbar A. D. (2017) The stable isotope geochemistry of molybdenum. *Rev. Mineral. Geochem.* **82**, 683–732.
- Koschinsky A. and Hein J. (2003) Uptake of elements from seawater by ferromanganese crusts: solid-phase associations and seawater speciation. *Mar. Geol.* **198**, 331–351.
- Kunzmann M., Halverson G. P., Sossi P. A., Raub T. D., Payne J. L. and Kirby J. (2013) Zn isotope evidence for immediate resumption of primary productivity after snowball earth. *Geology* **41**, 27–30.
- Lea D. W. (2014) 8.14 – Elemental and isotopic proxies of past ocean temperatures. In *Treatise on Geochemistry* (eds. K. K. Turekian and H. D. Holland), 2nd edition. Elsevier, Oxford, pp. 373–397.
- Lemaitre N., de Souza G. F., Archer C., Wang R.-M., Planquette H., Sarthou G. and Vance D. (2020) Pervasive sources of isotopically light zinc in the North Atlantic Ocean. *Earth Planet. Sci. Lett.* **539** 116216.
- Li Y.-X., Montañez I. P., Liu Z. and Ma L. (2017) Astronomical constraints on global carbon-cycle perturbation during Oceanic Anoxic Event 2 (OAE2). *Earth Planet. Sci. Lett.* **462**, 35–46.
- Little S. H., Vance D., Walker-Brown C. and Landing W. M. (2014a) The oceanic mass balance of copper and zinc isotopes investigated by analysis of their inputs and outputs to ferromanganese oxide sediments. *Geochim. Cosmochim. Acta* **125**, 673–693.
- Little S. H., Sherman D. M., Vance D. and Hein J. R. (2014b) Molecular controls on Cu and Zn isotopic fractionation in Fe-Mn crusts. *Earth Planet. Sci. Lett.* **396**, 213–222.
- Little S. H., Vance D., McManus J. and Severmann S. (2016) Critical role of continental margin sediments in the oceanic mass balance of Zn and Zn isotopes. *Geology* **44**, 207–210.
- Little S. H., Wilson D. J., Rehkämper M., Adkins J. F., Robinson L. F. and van de Flierdt T. (2021) Cold-water corals as archives of seawater Zn and Cu isotopes. *Chem. Geol.* **578** 120304.
- Liu S.-A., Wu H., Shen S.-Z., Zhang S., Lv Y., Zhang H. and Li S. (2017) Zinc isotope evidence for intensive magmatism immediately before the end-Permian mass extinction. *Geology* **45**, 343–346.
- Lohan M. C., Statham P. J. and Crawford D. W. (2002) Total dissolved zinc in the upper water column of the subarctic North East Pacific. *Deep-Sea Res. Part A* **49**, 5793–5808.
- Manheim F. and Lane-Bostwick C. (1991) Chemical composition of ferromanganese crusts in the world ocean: a review and comprehensive database. Open-File Report 89–020, U.S. Geological Survey, Woods Hole, MA.
- Marchitto T. M., Curry W. B. and Oppo D. W. (2000) Zinc concentrations in benthic foraminifera reflect seawater chemistry. *Paleoceanogr. Paleoclimatol.* **15**, 299–306.
- Marchitto T. M., Oppo D. W. and Curry W. B. (2002) Paired benthic foraminiferal Cd/Ca and Zn/Ca evidence for a greatly increased presence of Southern Ocean Water in the glacial North Atlantic. *Paleoceanogr. Paleoclimatol.* **17**, 10–11–10–18.

- Maréchal C., Nicolas E., Douchet C. and Albarède F. (2000) Abundance of zinc isotopes as a marine biogeochemical tracer. *Geochem. Geophys. Geosyst.* **1**, 1015.
- Maréchal C. N., Télouk P. and Albarède F. (1999) Precise analysis of copper and zinc isotopic compositions by plasma-source mass spectrometry. *Chem. Geol.* **156**, 251–273.
- Mavromatis V., González A. G., Dietzel M. and Schott J. (2019) Zinc isotope fractionation during the inorganic precipitation of calcite – towards a new pH proxy. *Geochim. Cosmochim. Acta* **244**, 99–112.
- Milliman J. D. (1974) Precipitation and cementation of deep-sea carbonate sediments. In *Deep-Sea Sediments. Marine Science* (ed. A. L. Inderbitzen). Springer, Boston, MA, pp. 463–476.
- Morel F. M. M. and Price N. M. (2003) The biogeochemical cycles of trace metals in the oceans. *Science* **300**, 944–947.
- Moynier F., Vance D. and Fujii T. (2017) The isotope geochemistry of zinc and copper. *Rev. Mineral. Geochem.* **82**, 543–600.
- Noé S., Titschack J., Freiwald A. and Dullo W.-C. (2006) From sediment to rock: diagenetic processes of hardground formation in deep-water carbonate mounds of the NE Atlantic. *Facies* **52**, 183–208.
- Peirce J., Weissel J., et al. (1989) *Proceedings of the Ocean Drilling Program, Initial Reports, 121*. College Station, TX.
- Pena L. D., Calvo E., Cacho I., Eggins S. and Pelejero C. (2005) Identification and removal of Mn-Mg-rich contaminant phases on foraminiferal tests: implications for Mg/Ca past temperature reconstructions. *Geochem. Geophys. Geosyst.* **6**, Q09P02.
- Penman D. E., Hönisch B., Zeebe R. E., Thomas E. and Zachos J. C. (2014) Rapid and sustained surface ocean acidification during the Paleocene-Eocene Thermal Maximum. *Paleoceanogr. Paleoclimatol.* **29**, 357–369.
- Pichat S., Douchet C. and Albarède F. (2003) Zinc isotope variations in deep-sea carbonates from the eastern equatorial Pacific over the last 174 ka. *Earth Planet. Sci. Lett.* **210**, 167–178.
- Pogge von Strandmann P. A. E., Jenkyns H. C. and Woodfine R. G. (2013) Lithium isotope evidence for enhanced weathering during Oceanic Anoxic Event 2. *Nat. Geosci.* **6**, 668–672.
- Poulton S. W. and Canfield D. E. (2005) Development of a sequential extraction procedure for iron: implications for iron partitioning in continentally derived particulates. *Chem. Geol.* **214**, 209–221.
- Romaniello S. J., Herrmann A. D. and Anbar A. D. (2013) Uranium concentrations and  $^{238}\text{U}/^{235}\text{U}$  isotope ratios in modern carbonates from the Bahamas: assessing a novel paleoredox proxy. *Chem. Geol.* **362**, 305–316.
- Samanta M., Ellwood M. J., Sinoir M. and Hassler C. S. (2017) Dissolved zinc isotope cycling in the Tasman Sea, SW Pacific Ocean. *Mar. Chem.* **192**, 1–12.
- Shimmield G. B. and Price N. B. (1986) The behavior of molybdenum and manganese during early sediment diagenesis – offshore Baja California. *Mar. Chem.* **19**, 261–280.
- Sieber M., Conway T. M., de Souza G. F., Hassler C. S., Ellwood M. J. and Vance D. (2020) Cycling of zinc and its isotopes across multiple zones of the Southern Ocean: insights from the Antarctic circumnavigation expedition. *Geochim. Cosmochim. Acta* **268**, 310–324.
- Siebert C., Nögler T. F. and Kramers J. D. (2001) Determination of molybdenum isotope fractionation by double-spike multicollector inductively coupled plasma mass spectrometry. *Geochem. Geophys. Geosyst.* **2**.
- Sweere T. C., Dickson A. J., Jenkyns H. C., Porcelli D., Elrick M., van den Boorn S. H. J. M. and Henderson G. M. (2018) Isotopic evidence for changes in the zinc cycle during Oceanic Anoxic Event 2 (Late Cretaceous). *Geology* **46**, 463–466.
- Tessier A., Campbell P. G. C. and Bisson M. (1979) Sequential extraction procedure for the speciation of particulate trace metals. *Anal. Chem.* **51**, 844–850.
- van Dijk I., de Nooijer L. J., Wolthers M. and Reichert G.-J. (2017) Impacts of pH and  $[\text{CO}_3^{2-}]$  on the incorporation of Zn in foraminiferal calcite. *Geochim. Cosmochim. Acta* **197**, 263–277.
- Vance D., Little S. H., Archer C., Cameron V., Andersen M. B., Rijkenberg M. J. A. and Lyons T. W. (2016) The oceanic budgets of nickel and zinc isotopes: the importance of sulfidic environments as illustrated by the Black Sea. *Phil. Trans. R. Soc. A* **374**, 20150294.
- Vance D., de Souza G. F., Zhao Y., Cullen J. T. and Lohan M. C. (2019) The relationship between zinc, its isotopes, and the major nutrients in the North-East Pacific. *Earth Planet. Sci. Lett.* **525** 115748.
- Viers J., Dupré B. and Gaillardet J. (2009) Chemical composition of suspended sediments in world rivers: new insights from a new database. *Sci. Tot. Environ.* **407**, 853–868.
- Voegelin A. R., Nögler T. F., Samankassou E. and Villa I. M. (2009) Molybdenum isotopic composition of modern and Carboniferous carbonates. *Chem. Geol.* **265**, 488–498.
- Wang R. M., Archer C., Bowie A. R. and Vance D. (2019) Zinc and nickel isotopes in seawater from the Indian Sector of the Southern Ocean: the impact of natural iron fertilization versus Southern Ocean hydrography and biogeochemistry. *Chem. Geol.* **511**, 452–464.
- Weber T., John S., Tagliabue A. and DeVries T. (2018) Biological uptake and reversible scavenging of zinc in the global ocean. *Science* **361**, 72–76.
- Zhang F., Algeo T. J., Cui Y., Shen J., Song H., Sano H., Rowe H. D. and Anbar A. D. (2019) Global-ocean redox variations across the Smithian-Spathian boundary linked to concurrent climatic and biotic changes. *Earth-Sci. Rev.* **195**, 147–168.
- Zhao Y., Vance D., Abouchami W. and de Baar H. J. W. (2014) Biogeochemical cycling of Zn and its isotopes in the Southern Ocean. *Geochim. Cosmochim. Acta* **125**, 653–672.
- Zhao M., Tarhan L. G., Zhang Y., Hood A., Asael D., Reid R. P. and Planavsky N. J. (2021) Evaluation of shallow-water carbonates as a seawater zinc isotope archive. *Earth Planet. Sci. Lett.* **553** 116599.

Associate editor: Weiqiang Li